

Evolving Physically Simulated Flying Creatures for Efficient Cruising

Yoon-Sik Shim
Chang-Hun Kim

Department of Computer Science
and Engineering
Korea University
Anam-dong 136-701
Seoul, South Korea
necromax@gmail.com
chkim@korea.ac.kr

Abstract The body-brain coevolution of aerial life forms has not been developed as far as aquatic or terrestrial locomotion in the field of artificial life. We are studying physically simulated 3D flying creatures by evolving both wing shapes and their controllers. A creature's wing is modeled as a number of articulated cylinders, connected by triangular films (patagia). The wing structure and its motor controllers for cruising flight are generated by an evolutionary algorithm within a simulated aerodynamic environment. The most energy-efficient cruising speed and the lift and drag coefficients of each flier are calculated from its morphological characteristics and used in the fitness evaluation. To observe a wide range of creature size, the evolution is run separately for creatures categorized into three species by body weight. The resulting creatures vary in size from pigeons to pterosaurs, with various wing configurations. We discuss the characteristics of shape and motion of the evolved creatures, including flight stability and Strouhal number.

Keywords

Virtual creature, body-brain coevolution, flapping flight, aerodynamics, avian power curve, flight stability, Strouhal number

1 Introduction

In recent years, a number of studies have been conducted on evolving both the morphology and locomotion of physically simulated virtual agents. Sims [43, 44] pioneered an innovative approach in generating both the morphology and the behavior of physics-based articulated figures by artificial evolution. His *blockies* creatures moved in a way that looked both organic and elegant. Other recent work, such as Sexual Swimmers [55], Framsticks [21], and Virtual Pets [35], has produced a range of applications. The Golem project [23] even took this technique a step further by evolving simulations of physically realistic mobile robots and then building real-world copies.

While the most recent work in this area [6, 20, 51, 56] has produced an assortment of virtual creatures crawling on the land or swimming under water, relatively little attention has been paid to the synthesis of flapping flight. Reynolds [39] developed a stochastic model of the flocking behavior of birds, but he did not animate individual birds. Ramakrishnananda and Wong [34] presented a physically based bird model using two segmented airfoils, but the entire motion of both wings is controlled by predesigned kinematics, and only the overall lift and thrust were calculated from aerodynamics. Wu and Popović [58] developed a realistic model of a bird with flexible feathers and successfully generated flying motions corresponding to given trajectories by optimizing the control parameters for each wingbeat, using simulated annealing. Augustsson et al. [2] conducted online learning by a real robot with flat wings to develop flying behavior using an evolutionary algorithm. Encouraged by these studies, we have proposed a new developmental model for evolving wing morphology and behavior using a traditional nested graph structure [41], and we have also attempted to exert high-level control over flying creatures using a neural network with a two-step

evolution strategy [42]. But our attempts to apply neural control to flight itself have not been successful, because of the intrinsic instability of the aerial environment. Its properties are significantly different from those of the land or water.

One of the crucial points in evolving virtual creatures with simulated physics is the sensitivity of locomotion. Sensitivity can be considered as the ease with which a creature's locomotion can be interrupted, or even terminated, by external or internal disturbances. External disturbances come from the surroundings, and might include gusts of wind or unexpected obstacles. Even without these effects, generating the basic locomotion of a linked body structure would be a challenging problem in itself. Internal disturbances are unexpected changes caused by the movement of the creature itself, such as vortices and turbulence in the fluid, and inertial forces during maneuvering. A common but important external influence is gravity. Because of the existence of gravity, a creature in motion also needs to retain its balance to maintain stable locomotion by exploiting hydro/aerodynamic forces from the fluid medium or counteractive/frictional forces from the ground.

Underwater is a more stable environment. Water has a higher density and viscosity than air, so the motion of an immersed body is less sensitive to disturbances. Moreover, buoyancy greatly reduces the effect of gravity. Underwater creatures have less need to balance, and can adopt an almost arbitrary attitude. For land creatures, balancing problems are related to factors such as the height of their center of mass, the number and configuration of their legs, and terrain irregularity. Terrestrial creatures that fail to maintain balance will fall over, and locomotion will terminate immediately. Even creatures for which balance is less important, such as snakes and creeping insects, need to adapt attitudes appropriate for their direction of motion; for instance, many animals cannot move if they are turned over or laid on their side.

Maintaining locomotive stability in the air is much tougher than in these other two environments. The density and viscosity of the surrounding medium is much lower than that of the water, and there is little buoyancy and nowhere to stand. And a failure of locomotion can mean the death of the creature. The interaction between a flapping wing and the air is very complicated. The forces generated by this interaction are chaotic, and their simulation is often unstable because of high sensitivity. Computational fluid dynamics (CFD) methods are sufficiently accurate, but too time-consuming to build into an evolution framework. For instance, Milano et al. [25] conducted a CFD study using a controlled random search genetic algorithm to optimize the placement and operating parameters of two actuator systems (rotating surface belts and jet actuators) on a single cylinder in order to reduce the drag coefficient. The optimized cases showed over 50% drag reduction. However, their simulation took up to 1500 iterations to converge, requiring 30 hours of CPU time on an NEC SX-4 supercomputer, making their approach computationally very intensive.

In this article, we focus on evolving structure and control for stable and efficient cruising flight, as a preliminary to addressing in-flight maneuvers. This work begins with a neutral state of locomotion, which must be mechanically efficient and stable. The avian power curve [27, 28, 37], with its characteristic U shape, plays a central role in defining the scope of our work. This curve shows how power varies as a function of flight speed, summarizes the most important aspects of flight performance and stability [49, 53], and has proved to be a valuable tool for understanding many of the decisions that flying animals make in flight. It is also strongly related to the physical and morphological properties of flying animals, so that it can offer valuable knowledge about the body-brain coevolution of flight. We use the avian power curve to achieve optimal flight speeds with minimum power consumption. Aerodynamic stability is considered in the fitness evaluation by measuring force and moment equilibrium, and additional passive stabilization is considered by varying the point at which the wing is attached to a creature's body.

The rest of this article is organized as follows: In Section 2, we overview the physical structure of a creature and its controller and introduce an encoding scheme that can express this data as a genotype. We describe simplified conventional aerodynamics for the aerial environment in Section 3. Section 4 deals with extracting the desired flight speed from an avian power curve and the physical properties of a creature. Section 5 describes fitness evaluation and the evolution process. We present

our results in Section 6 and discuss flight stability in cruising by means of experiments which introduce external disturbances. We also discuss the physical validity of our work by investigating the Strouhal numbers of evolved flyers and comparing them with those of real birds.

2 The Model

Our creatures are constructed from a basic model with truss-shaped wings [41, 42]. This design is inspired by the hang glider and the bat wing. We have simplified and generalized this idea into an arbitrarily constructible wing skeleton, which we can use to explore various wing structures beyond those known in nature.

As shown in Figure 1, genotype encoding is accomplished using a multiconnected list, which assesses symmetry of shape and wing motion. Handling variations of the genotype, such as mutation or mating, is convenient because of this linear structure. The root node represents the body of a creature, and the wing root represents the start of the wings, at a point inside the central body. These first two nodes and their connections exist in all individuals, but are followed by an arbitrary number of wing segment nodes. A tail also exists as a fan-shaped surface, and its radius is included in the genotype description. The angle of the fan (tail spread) is fixed at 22.5° . In this current work a tail only exerts small forces, but it is likely to become more important when maneuvers are considered.

2.1 Creature Development

A creature's skeleton is made from capped cylinders, each of which is aligned along a local z axis. A wing joint connects a child cylinder to its parent and can have one or two degrees of freedom, allowing both dihedral and sweep motions. The parameters of each cylinder are contained in the corresponding node in the genotype description. The centers of the hemispherical ends become the start and end point of a cylinder. The start point is position 0, and the end point corresponds to a specified parametric distance along the cylinder's local z axis.

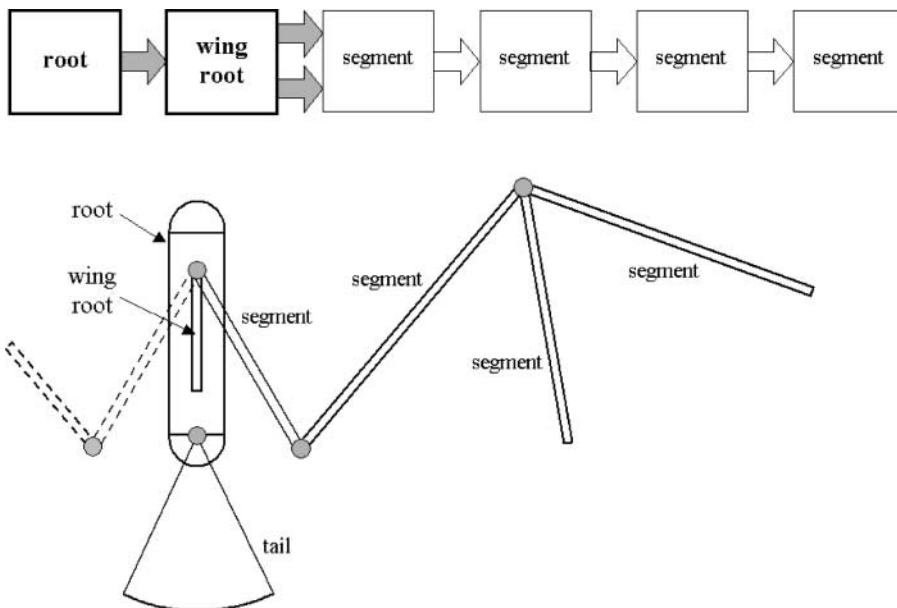


Figure 1. A genotype and a creature structure. Each node of a genotype contains the cylinder parameter (length, radius, joint type, and a motor controller). The radii of the wing root and the following segments are all fixed to the same value. Each connection has parameters that indicate how two body parts should be connected (position and orientation).

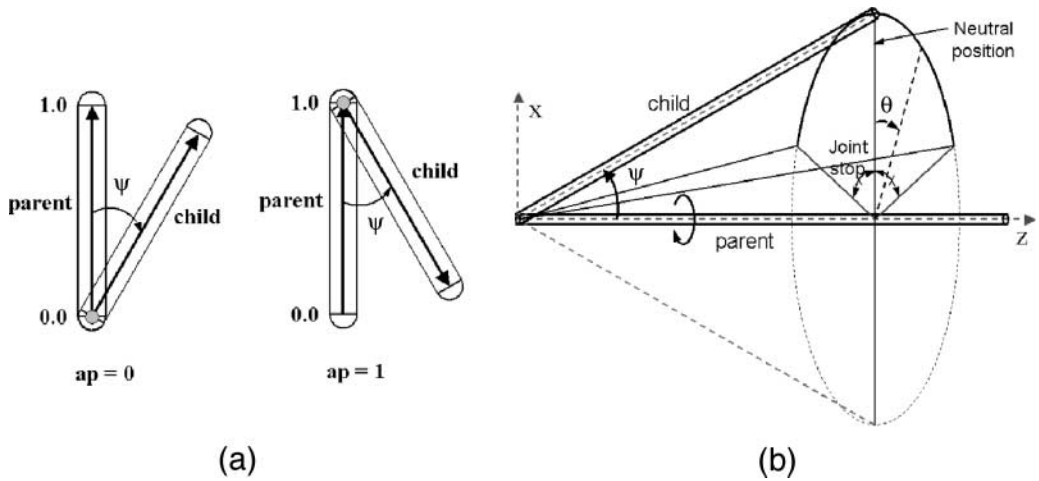


Figure 2. Joining a cylinder pair. (a) Initial arrangement of cylinders. If the attachment point (**ap**) flag is 0, the child cylinder rotates through an angle Ψ about the parent cylinder. If it is 1, the orientation of the child is flipped before rotating. (b) A dihedral joint rotates about the parent's local z axis (θ), and a sweep joint rotates in the Ψ direction.

A node connection specifies how and where to attach a cylinder to its parent. As shown in Figure 2, the connection parameter **ap** indicates the position on a parent cylinder where the child's 0 point will be placed, and by setting values of **ap** to 0 or 1 we obtain a trusslike wing structure. The angle between the local z axes of parent and child is ψ (limited to the range 10° to 90°), and this determines the direction in which the wing grows. θ is initially set to zero, so that the wings are aligned horizontally. ψ and θ are initialized to neutral values at each joint and changed over time by angular motors during the simulation. Figure 3 shows an example of this construction process, resulting in the wing skeleton shown in Figure 1.

Many studies on legged robots have used passive dynamics [54] and static stability [8] to construct efficient and robust locomotion. Several aeronautical studies [9, 26] have discussed static stability,

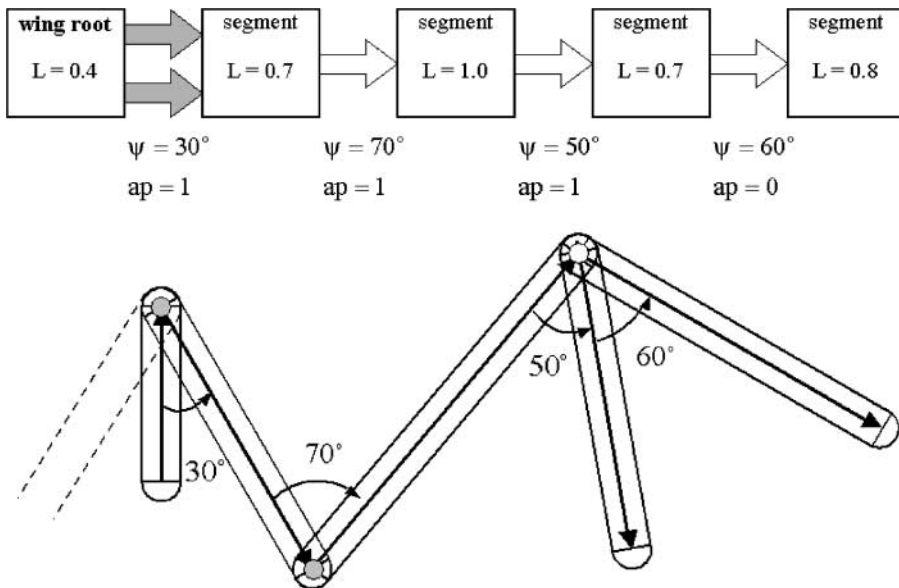


Figure 3. Detailed description of the skeleton construction shown in Figure 1.

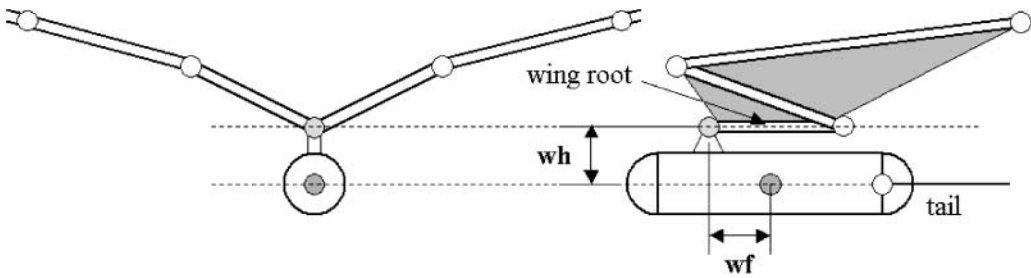


Figure 4. Relative position of the wing root and the body.

which produces stabilizing moments against external perturbations. Often, this process can be helped by proper location of the relative position of the wing root and body. Figure 4 shows two variables \mathbf{wh} and \mathbf{wf} , which describe the horizontal and vertical distance of the wing root from the body's center of mass. This helps the creature to stabilize pitch and roll movement. The range of each value is $[0, 2R]$ for \mathbf{wh} and $[-0.4L, 0.4L]$ for \mathbf{wf} , where R and L are the radius and length of the body. This will be discussed in more detail in Section 6.

After two cylinders have been attached to each other, a weightless rigid film, forming a patagium, is stretched between them. Figure 5 shows an example of a complete creature. Since each triangle of film is attached to a child cylinder, its linear and angular velocities can be calculated from those of the child cylinder. The whole of a creature's wing, looking like that of a bat or hang glider, is composed of a sequence of child-parent pairs with attached triangles of film, each of which is subject to appropriate aerodynamic forces.

2.2 Controller

Although continuous-time neural networks (CTRNNs) are widely used in robot control [4, 5, 11, 45] and can generate a variety of signal patterns, the use of a periodic sinusoidal function has advantages for the purposes of this work. Most continuous locomotion of real animals (especially in flapping flight) can be expressed in terms of the harmonics of sinusoidal functions. A sinusoidal function has infinite derivative continuity, so that unexpected fluctuations of the joint motors, which might be critical disturbances in flight, can be minimized. However, expressing a single motor signal using sinusoidal harmonics needs many parameters, and the search space of possible signal patterns then becomes unnecessarily huge (in effect it encompasses almost all wave patterns). Instead, we have chosen a piecewise composition of sinusoidal functions, which connects each piece smoothly.

Each controller specifies the angle to be achieved by a motor. The difference between the actual joint angle and the controller output is fed to the motor as a desired velocity. All controllers operate

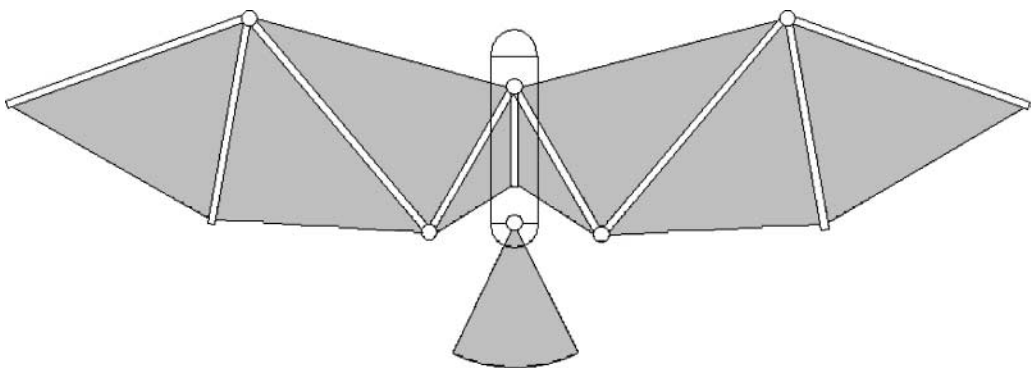


Figure 5. An example of a completed creature.

with a cycle of the same duration, so that all joint motions are controlled synchronously. The controller parameters include the duration of a cycle (T) and a number of control points that determine the shape of its output function. Each control point has a magnitude in the range $[-1,1]$ and a phase fraction in the range $[0,1]$, which represents the proportion of the cycle affected by this control point. The actual values of u are scaled by the joint range ($\pm \pi/2$ in this work), and those of t are scaled by the cycle period T . The control function is constructed by smooth interpolation between each pair of neighboring control points. In an interval $[t_n, t_{n+1}]$, we can write the controller function U as

$$U(t) = \frac{u_n + u_{n+1}}{2} + \frac{u_n - u_{n+1}}{2} \cos\left(\frac{t - t_n}{t_{n+1} - t_n} \pi\right), \tag{1}$$

where u is the output value of a control point, and t is the time parameter. Thus, $P(t, u)$ in Figure 6 is a graph of time against output in a 2D parameterized control space. The final control point is connected back to the first one, making the function periodic. These parameters are also coded into each node of the genotype.

3 Physics Simulation

The Open Dynamics Engine, an open-source simulator by Russell Smith [46], has been used to simulate the movement of a physical creature with articulated rigid body dynamics. The forces on the patagium are calculated by simplified aerodynamics. The simulation uses a first-order semi-implicit integrator, where the constraint forces are implicit and the external forces are explicit [1, 48].

The forces acting on a surface depend on its area and the angle of attack with respect to the velocity of the airstream. Since this work deals with large flying creatures (at least bird size), it is reasonable to use a conventional aerodynamics. We used blade element theory with a quasi-steady assumption [57] as the simplified aerodynamics.

The triangular element of a patagium covering a parent-child cylinder pair is divided into several patches, and the calculated forces are considered to be exerted on the center of mass of each patch. The stream velocity for each patch is calculated by inverting the sign of the vector representing the

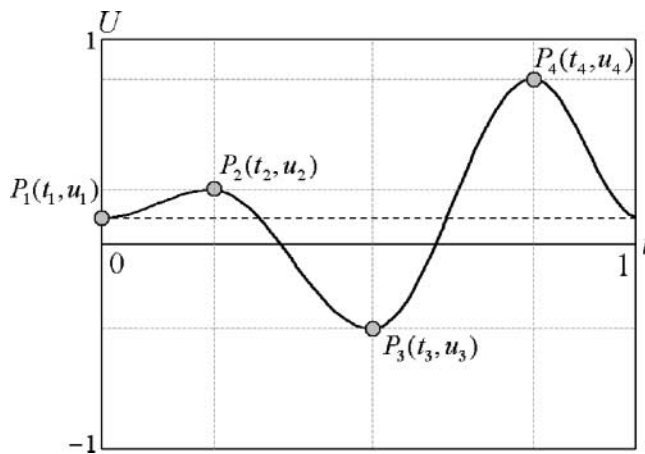


Figure 6. An example of a parameterized control function.

velocity of the patch’s center of mass and projecting it onto the plane formed by the patch’s normal and the local z axis. The lift and drag forces can then be calculated using the lift coefficient C_L and the drag coefficient C_D . The lift coefficient is proportional to the angle of incidence (α) of the wing, and, from thin-airfoil theory [12], its slope is 2π for a 2D wing of infinite span. However, Prandtl’s lifting-line theory [32, 33] shows that for a finite span, the slope depends on the aspect ratio of the wing because of the effect of induced velocity. In Prandtl’s model, the drag coefficient C_D is composed of induced and parasite components, and yields an airfoil polar equation of the form

$$C_D = C_{D_0} + \frac{C_L^2}{\pi\epsilon(AR)}, \tag{2}$$

where

$$C_L = 2\pi\left(\frac{AR}{AR + 2}\right)\alpha. \tag{3}$$

C_{D_0} is the parasite drag coefficient due to viscosity, and is assumed to be 0.1; ϵ is the Munk span efficiency, which is normally slightly less than 1 (we set it to 1); and AR is the aspect ratio determined by $AR=4b^2/S$. However, α cannot be very large, because flow separates and the wing stalls at high angles of attack. In reality, if the angle of attack increases and passes the stall angle, at one point all lift will be lost while the drag continues to increase. We therefore modeled the shape of the lift coefficients, as shown in Figures 8 and 9, by synthesizing functions to return lift coefficients for any given angle. (The maximum value is proportional to AR ; for $AR = 7.25$, the value is 1.6.) The line is shifted to the left so that a zero angle of attack corresponds to $\alpha_0 \approx -4^\circ$. The drag coefficient is generated using Equation 2 over the active range of the lift coefficient, and gradually flattened to 2 near $\pm 90^\circ$. Drag acts in the direction of the airstream velocity. The direction of lift is

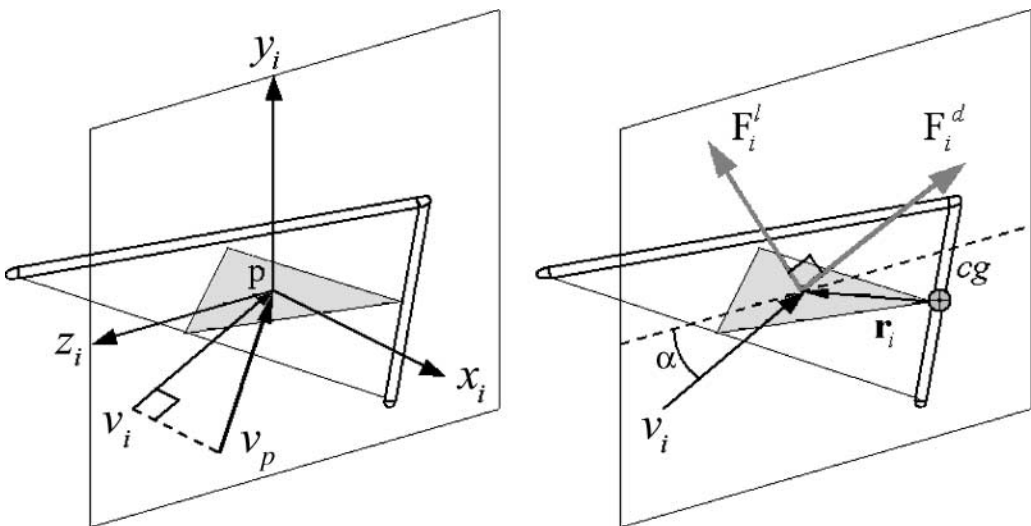


Figure 7. Force on a triangular patch i , with local axes x_i , y_i , and z_i . The actual air velocity (v_i) is projected onto the patch’s local yz plane, and the resultant vector v_p is taken as the incoming velocity. Initially, the local axes of patches are those of the central body.

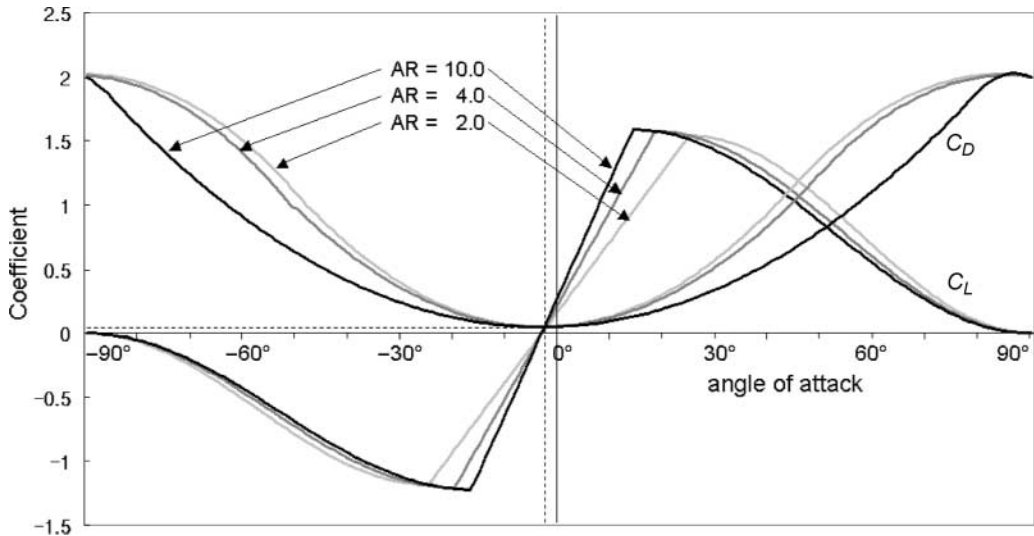


Figure 8. Lift and drag coefficients. A wing with high aspect ratio (AR) receives more lift and less drag.

perpendicular to that of the drag, so a patch produces not only lift but also thrust tangential to its surface (Figure 7). The force on each patch i is returned to the physics simulator as an accumulated force on the child cylinder:

$$\mathbf{F}_{L,i} = \frac{1}{2} \rho C_L(\alpha) S_i ||\mathbf{v}_i||^2 \mathbf{l}_i, \tag{4}$$

$$\mathbf{F}_{D,i} = \frac{1}{2} \rho C_D(\alpha) S_i ||\mathbf{v}_i||^2 \mathbf{d}_i, \tag{5}$$

where S is the area of the patch, and ρ is the density of the air (1.21 kg/m^3). After the forces on each patch have been calculated, the resulting force and the torque on the cylinder are obtained by

$$\mathbf{F}_{\text{total}} = \sum_{i \in N} \mathbf{F}_{L,i} + \mathbf{F}_{D,i}, \tag{6}$$

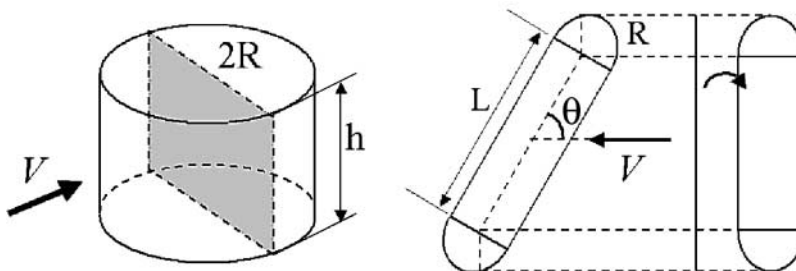


Figure 9. The area of a cylinder projected onto the stream direction.

$$\mathbf{T}_{\text{total}} = \sum_{i \in N} (\mathbf{F}_{L,i} + \mathbf{F}_{D,i}) \times \mathbf{r}_i, \tag{7}$$

where N is the set of patches in the triangular segments, and \mathbf{r} is a vector from the cylinder’s center of mass to the center of the each segment. The forces on the tail can be calculated in the same way as those on a wing patch. The angle of the tail fan is fixed at 22.5° .

The parasite drag on the central body cylinder is also calculated using Equation 5, and can be written as

$$\mathbf{F}_D = \frac{1}{2} \rho C_{db} (2RL \sin \theta + \pi R^2) \mathbf{v} \mathbf{v}, \tag{8}$$

where $C_{db} \approx 0.1$ is the body drag coefficient. As shown in Figure 9, the area that receives this force is idealized as the projection of the capped cylinder onto a surface normal to the velocity vector.

4 The Avian Power Curve

The avian power curve, with its characteristic U shape, shows how power varies as a function of flight speed. It summarizes the most important aspects of flight performance, and has proved to be a valuable tool for understanding many of the strategies of flying animals. From the geometry of the power curve, or by simple manipulations of the underlying mathematical models, it is possible to make predictions about, for instance, choices such as the selection of flight speed in relation to wind, food availability, or a migration goal [15, 16], or decisions between steady and intermittent flight [36, 38].

Birds and other flying animals can fly at a variety of speeds, and their flapping kinematics may change with speed. Our primary interest is to observe common and energy-efficient wing motions by the evolved creatures, rather than simple gliding or hovering in the air with laborious wingbeats. In this work, we have adopted a power curve obtained from a mathematical model by Pennycuik [27, 47], and we set the creatures to fly near to the minimum-power speed of their individual power curves. The total mechanical power, P , required for flight is calculated as

$$P = P_i + P_{\text{par}} + P_{\text{pro}}, \tag{9}$$

where P_i is the induced power required to support the weight, P_{par} is the parasite power required to overcome viscous drag on the body, and P_{pro} is the profile power required to overcome viscous drag on the wing surface. The general shape of the power curve can be expressed in the form $P = 1/V + V^3$, which has a characteristic U shape (Figure 10). We can obtain V_{mp} by differentiating the power equation $\frac{\partial P}{\partial V} |_{V_{mp}} = 0$ and rewriting V_{mp} as

$$V_{mp}(m, b, S_b) = \left(\frac{\kappa g^2}{3\pi \rho^2 C_{db}} \right)^{\frac{1}{4}} \left(\frac{m^2}{b^2 S_b} \right)^{\frac{1}{4}} = K \left(\frac{m^2}{b^2 S_b} \right)^{\frac{1}{4}}. \tag{10}$$

In this equation, κ (≈ 1.2) is the airfoil efficiency factor, S_b is the frontal area of the body, and C_{db} (≈ 0.1) is the body drag coefficient. The complete derivation of these equations is presented elsewhere [47]. From this approximation, V_{mp} is represented as a function of mass and shape. We set K as a proportional factor, and its calculated value is 3.0246. Table 4 in Section 7 shows the morphological parameters and calculated V_{obs}/V_{mp} for various species of birds, collected from [29–31].

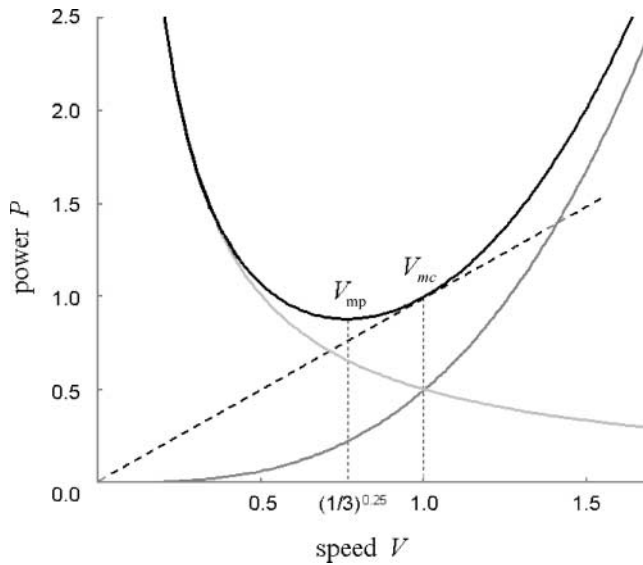


Figure 10. The idealized lifting-line power curve. This is shown in nondimensional form, together with induced ($\frac{1}{2V}$) and friction ($\frac{1}{2}V^3$) terms. This curve yields two characteristic speeds: V_{mc} is the speed at which the tangent from the origin meets the curve, and at which the cost of transport is a minimum [37]; and at V_{mp} , the power consumption is a minimum.

Pennycuik [30] indicated the relation between V_{mp} and observed flight speeds. From the data in Table 4, V_{obs}/V_{mp} can be described as a function of mass;

$$\frac{V_{obs}}{V_{mp}} = 0.9868 - 0.2706 \log m. \tag{11}$$

Figure 11 illustrates this approximation by showing V_{obs}/V_{mp} plotted against $\log m$. This indicates that smaller birds usually fly faster than their minimum-power speed.

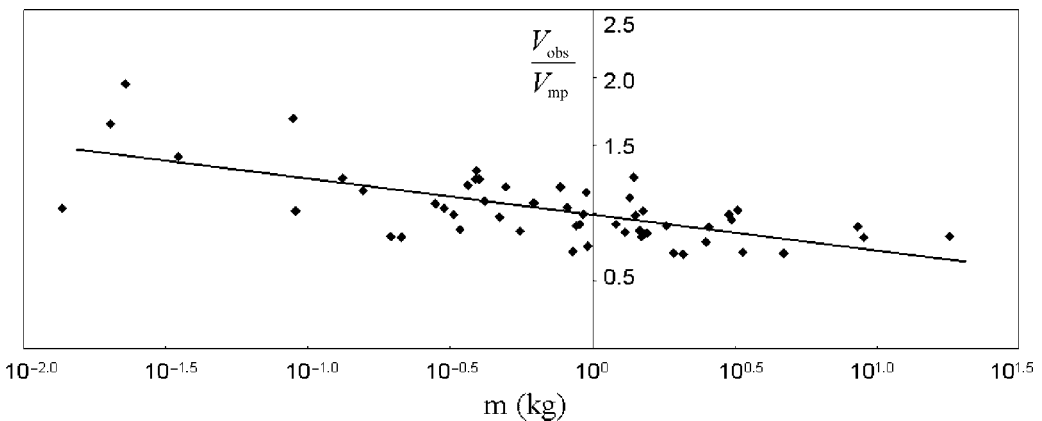


Figure 11. Logarithmic plot of the ratio of the observed speed V_{obs} to the calculated minimum-power speed V_{mp} , obtained from Pennycuik [29–31].

5 Evolution Process

We divided our creatures into three species based on their mass (small, medium, and heavy), and the simulation was run separately for each category. The creature’s body density was set to 300 kg/m^3 , a careful heuristic choice to match the body size and the overall mass of the creature. We roughly set the limits of other morphological data, such as wing load and aspect ratio, within the acceptable range. Table 1 shows the parameter ranges used in the simulation.

5.1 Fitness Evaluation

Each creature was rewarded for a long flight time and for high flight speed in the forward direction, and penalized for high vertical acceleration of the center of mass (disequilibrium between gravity and lift), high angular acceleration (reduced aerodynamic moment), and high torques at the joint motors (power consumption). The creature receives no extra reward for speeds higher than V_{mp} . This is because the maximum available motor torque is not explicitly constrained. It would be possible to assign different cylinder radii and maximum torques to each of them [44], but it is hard to make a creature with such a thick skeleton fly, and a factor to determine the actual torque value has to be carefully tuned. Providing a high torque means that the creature can fly extraordinarily fast (using “superpower”), and this will result in fast flapping flight like that of a dragonfly at very high velocities. Criteria other than speed of flight are used to differentiate between creatures flying at speeds around V_{mp} . The fitness function is

$$f_{\text{tot}} = k_b \frac{t_b}{T} + (2 - k_b) \frac{1}{\sum k_i} \sum_t^T f(t), \tag{12}$$

Table 1. Some of the parameter settings.

Parameter	Value		
	Small	Medium	Heavy
Total mass (kg)	0.02–0.7	0.1–10.0	10.0–50.0
Number of wing segments	4–10	4–10	4–10
Central body length (m)	0.02–0.2	0.2–0.8	0.5–1.0
Central body radius (m)	0.1L–0.3L	0.1L–0.3L	0.1L–0.3L
Wing segment length (m)	0.002–0.1	0.02–0.5	0.3–1.5
Wing segment radius (m)	0.005	0.01	0.01
ψ (rad)	0.2–1.5	0.2–1.5	0.2–1.5
Wingbeat frequency (Hz)	1.0–20.0	1.0–8.0	0.5–4.0
Number of control points	1–4	1–4	1–4
Simulation step (s)	0.005	0.01	0.02
Starting altitude (m)	10.0	20.0	40.0

$$f(t) = k_1 \zeta\left(\frac{V(t)}{V_{mp}}\right) + k_2 \frac{1}{1 + \Re(a_v(t))} + k_3 \frac{1}{1 + \|\alpha(t)\|} + k_4 \frac{1}{1 + \frac{1}{m} \sum^N \Gamma_i(t) \delta t}, \quad (13)$$

where f_{tot} is the total fitness, $f(t)$ is the fitness measured at time t , k_b is the fractional contribution of flight time, t_b is the maximum flight time, T is the total evaluation time, V is the forward speed, a_v is the vertical acceleration of the center of mass of the creature, α is the angular acceleration of the central body, m is the mass of the creature (a heavier one may use more torque in absolute value), Γ_i is the torque of the i th motor, N is the number of motors, and δt is the time step. $\zeta(x)$ is equal to x when $x < 1$, otherwise 1. $\Re(x)$ is $-2x$ when $x < 0$, otherwise x . This attaches more penalty to downward acceleration (falling). The values of k used were $k_b = 0.9$, $k_1 = 1.2$, $k_2 = 1.2$, $k_3 = 1.2$, $k_4 = 1.0$.

5.2 Evolutionary Algorithm

Using a typical evolutionary algorithm tends to apply a strong selection pressure to creatures and leads to premature convergence. To ensure genetic diversity, a geographically distributed genetic algorithm [17] was used, usually with a population of 400 (20×20 grid) individuals. Within the grid core lies the concept of a neighborhood. The child is placed at a position near its parents, so it is possible for two different solutions of equal fitness to exist as demes on different parts of the grid. This can prevent the evolution process from reaching a local optimum in which the gene pool contains only one solution and the process is thus incapable of reaching a high fitness.

Mating was limited to the 8 grid squares surrounding a genotype, plus a 25% chance of it occurring within the next ring of 16 squares (see Figure 12). The algorithm for mating is as follows: first, a parent is chosen by tournament selection from three randomly chosen genotypes. From within the selected genotype’s neighborhood, three more genotypes are chosen. The best of these is mated with the selected genotype, and the worst is replaced by their offspring. A generation is completed when this process has been applied to a certain number of individuals. To implement elitism, the best individual in the population is selected 20% more frequently than the others. This procedure is shown graphically in Figure 13.

Using a square grid, the individuals at the corners or edges find it hard to propagate their genetic information to the other sides. To give them a better chance of mating, we used a wrapped form of 2D grid, as shown in Figure 12. The opposite edges are connected, and topologically the grid forms a torus. This allows every individual to have an equal number of neighborhoods. For the recombining process, both the double point crossover and grafting [43, 44] were used, with the same probability.

After mating, the offspring has a chance to mutate. The mutation rate was initially set to 0.5 and slowly reduced during evolution. Each genotype has its own adaptive mutation rate, which is

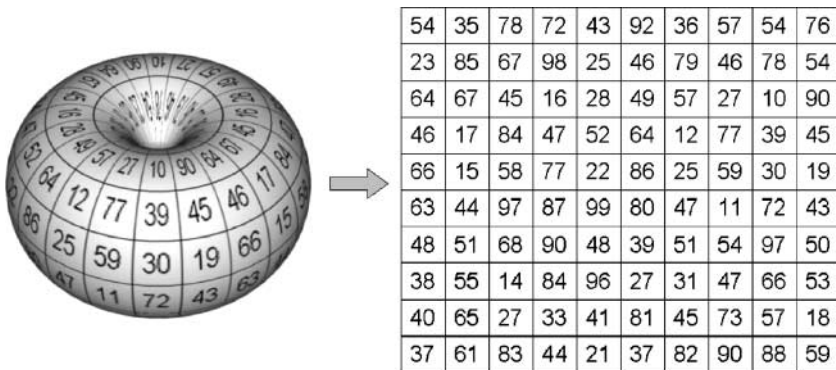


Figure 12. Population grid with toroidal geometry. A toroidal grid ensures that every individual has an equal number of neighborhoods.

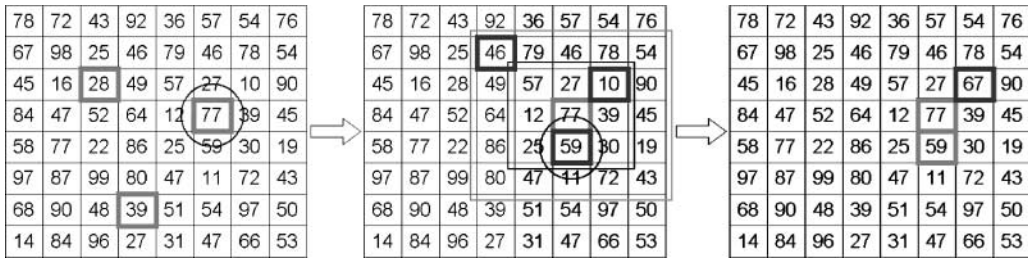


Figure 13. Grid-based mating scheme. First, three genotypes are chosen at random and the best is selected (parent 1). Second, three candidates for mating are selected within the surrounding 24 squares, and the best is chosen (parent 2). Finally, the worst of the three spouses is replaced by the offspring of parent 1 and parent 2.

adjusted every time mating occurs. If individuals A and B produce child C by mating, the mutation rate of C becomes the average of A and B’s mutation rates. If the fitness of C is greater than 70% of A and B’s average fitness, then A and B’s mutation rates are increased by ϵ ($=0.001$); otherwise they are reduced by ϵ . This design choice was inspired by studies in which bacteria appear to increase their mutation rate in stressful environments [40]. Over time the mutation rate of the parent is adjusted in an attempt to keep the children’s fitness at least 70% of their parents’. After adjusting the mutation rates, each genotype was mutated in the following steps:

1. The unique parameters such as wingbeat cycle, wing attachment point, or tail length have a chance of being mutated.
2. A new random node is added, or an existing node (other than the central body and the wing root) is deleted.
3. The internal parameters of each node have a chance of being subjected to alterations. Morphological parameters can be varied within their allowed range, and joint types are changed from one to another.
4. After changing the degrees of freedom of a joint, its controller parameters are mutated. A new control point is added or an existing one is deleted. Then the position of each control point is altered within its possible range.
5. The parameters of each connection are mutated.

When mutating the time fraction corresponding a control point, two points cannot be moved too close. That might result in a step change in motor velocity with a resulting peak in motor torque. Control points are not permitted to be closer than 10% of the total wingbeat duration.

The time required for the evaluation process as a whole was reduced by early termination of any individual that is not performing well. Creatures with mutually intersecting wings are replaced by a random individual. A creature is considered to be nonviable if the speed of any of its body parts exceeds a limit (typically 1000 m/s). Interim fitness measurements are performed after a quarter of the total evaluation period has elapsed, and any individuals whose fitness is less than one-fifth of that of the least fit creature of the previous generation are removed.

Additional checks were made for morphological errors corresponding to eccentric shapes that stray far from the range of wing loadings and aspect ratios that are characteristics of feasible flight. Wing loading is defined as the mass of the creature divided by its wing area, and the unit g/cm^2 is generally used. We used a range based on real-life data [13, 14, 24]. The permitted range of wing loading is 0.1 to 0.5 for the small, 0.3 to 1.0 for the medium, and 0.5 to 1.5 for the heavy creatures; while the aspect ratio should be 1 to 20 for small creatures and 3 to 20 for both medium and heavy. Any creature that is out of its range receives a negative score corresponding to the extent of its deviation. It is given no stronger penalty, so as to keep its other, potentially good features within the

population. Another kind of dynamic wing collision caused by a wide range of dihedral motion (*clapping*) was checked for, and if it was found, the creature's fitness was lowered by half. The statistics of the abnormal individuals are shown in Figure 15.

6 Results and Discussion

Each creature was placed at an initial altitude, and given an initial velocity of V_{mp} . The evaluation period was about 40–50 seconds in simulation time, representing between 100 and 500 generations. Most of the creatures used the dihedral joint of the wing segment nearest to the wing root to generate primary lift and thrust. The fitness of the population was dominated by flight time in the early stages of evolution. After the average flight time of all individuals reached a certain level, other fitness scores such as speed, force equilibrium, and efficient use of power took a greater role. Not all creatures are simulated for a full evaluation period: those that crash are deemed not to have useful genetic material and are terminated early.

Since individuals are evaluated while staying airborne, the duration of flight is crucial for survival through the early stages of evolution. In most simulations, a *jump* in fitness is observed, at which point the average flight time of the population achieves a stable value. If the contribution of flight time is reduced, the jump appears later in the total evaluation period. Many individuals get a high fitness score initially, but quickly crash. In this case, “high fitness during short lifetime” is recorded. We set the contribution of flight time to more than a quarter of the total fitness score ($0.7 < \kappa_f < 1.0$). The total fitness and the sub-scores are plotted as a function of the generation in Figure 14.

Emphasizing flight time promotes the ascendancy of creatures that can perform stable gliding. But these are passive solutions, without joint movement, so they cannot avoid losing speed and altitude. Solely in terms of performance, the difference between these gliders and successful flyers is unfortunately perceptible only over a long evaluation. We addressed this problem by forcing all creatures to have at least one pair of oscillating control points in at least one controller.

The starting altitude was adapted to the creature's wing loading, because light wing loading makes remaining aloft easier. The starting altitude was set as a function of wing loading within the prescribed range for each species:

$$\text{altitude} = \frac{2H}{W_{\min} + W_{\max}} w, \quad (14)$$

where H is the altitude where the wing loading is the middle value of the range, and its value is 5 m for the small, 10 m for the medium, and 20 m for the heavy creatures. W_{\min} and W_{\max} are the minimum and maximum wing loading, and w is the wing loading of the current individual. Figures 15 and 16 shows the best four creatures of each species; the detailed specification of each creature is presented in Table 2.

Disappointingly, there was no significant difference of wing shape between species, except that the medium and small creatures have wings that are somewhat more backward swept. Possible wing shape characteristics are: the aspect ratio, rounded or sharp wingtips, and forward, backward, or neutral sweep of wing. In this work, smaller wings tended to have high aspect ratio, but other differences cannot be captured. Our wing model cannot represent a smoothly rounded wingtip. Although the wingtip vortex is reflected in some extent in the model, it is not deeply modeled enough to affect the wingtip shape. Rather, it affects the aspect ratio and lift coefficient. We expect that wing sweep would be more clearly distinguished if the evolution were based on maneuvering flight. Generally, rapidly turning birds have wings with a backward sweep, and slow-turning birds have comparatively flat wings (Table 3).

However, there were differences in wingbeat frequencies, although the ranges for the species overlapped. The larger species had lower frequencies, though the medium and the small creatures did not have as high frequencies as we expected. Wing loadings were distributed near the lower

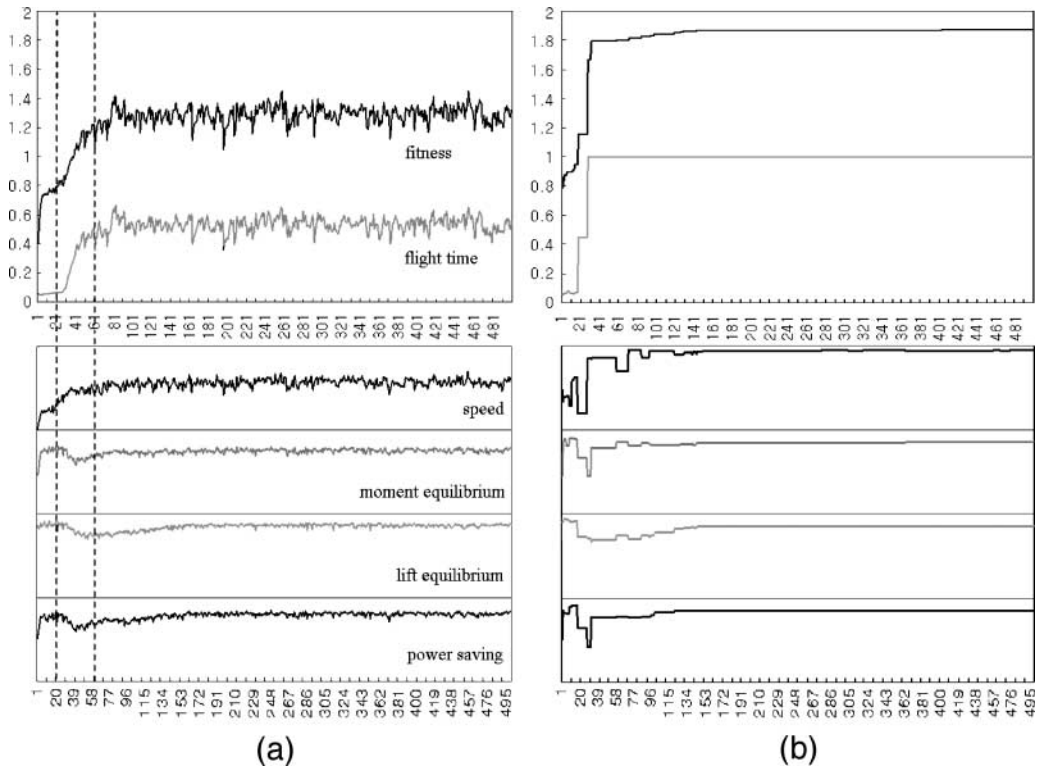


Figure 14. Fitness of the average (a) and the best individual (b) by generation. The period between the dashed vertical lines indicates a fitness jump. The scores for lift-weight equilibrium, moment equilibrium, and powerless flight become lower as the creatures start to flap their wings to stay in the air, and then gradually increases as efficient flight is achieved.

bounds in the given ranges. Flight speeds were higher for heavy creatures, as expected [52]. It seems that an isometric relation overlooks additional metabolic characteristics such as differences in respiratory system and chemical energy consumption. A more accurate relation might be obtained by relating the maximum available torque at each motor to the weight of the connected body parts, but such a relationship would need to be carefully tuned.

Despite these shortcomings, most creatures showed elegant flapping motions, and some folded their wings efficiently on the upstroke (see Figure 17b, motor 8). The creatures' flight is shown more fully in Figures 24, 25, and 26 (Section 7). There are also some movie clips and colored figures of this article available at <http://kucg.korea.ac.kr/~ysshim/shim/efcec.htm>.

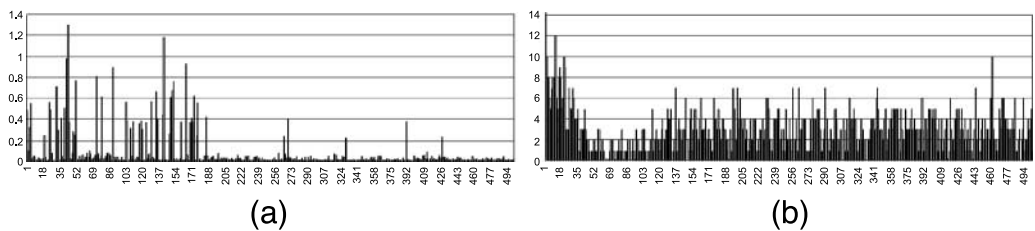


Figure 15. The numbers of creatures with (a) morphological errors (outranged wing loading or aspect ratio) and (b) clapping wings. Morphological errors decrease significantly after a while. Clapping creatures show less variation as evolution proceeds. While clapping is related to implementation of the simulation, the morphological error directly influences flight performance, although its effect is moderate.

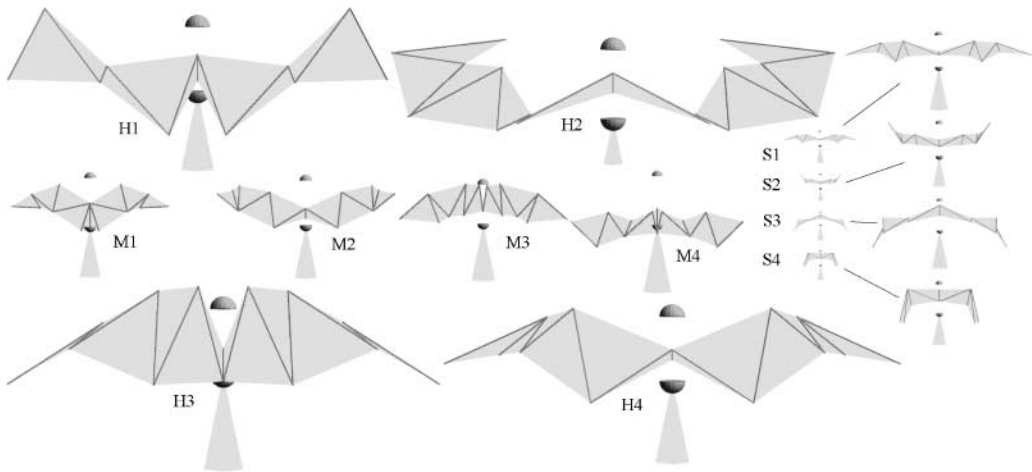


Figure 16. Some of the best-adapted creatures. H1 to H4 are heavy, M1 to M4 are medium, and S1 to S4 are small. The size ratio of the creatures is shown, but S1 to S4 are scaled and redrawn for clarity.

Table 2. Specification of evolved creatures.

Name	Mass (kg)	Wing area (m ²)	Half span (m)	Wing loading (g/cm ²)	Aspect ratio	Frequency (Hz)	Average speed (m/s)	V_{mp} (m/s)
H1	15.268	2.963	2.433	0.515	7.993	1.136	15.0	13.968
H2	16.920	3.197	2.825	0.529	9.981	0.806	14.0	13.564
H3	18.275	3.465	2.754	0.527	8.758	1.000	15.0	13.910
H4	16.710	3.138	2.911	0.532	10.798	1.250	13.5	13.124
M1	2.579	0.566	0.989	0.455	6.904	1.923	12.0	13.220
M2	2.766	0.685	1.128	0.404	7.431	2.083	14.0	12.423
M3	2.360	0.670	1.060	0.353	6.711	2.083	12.0	12.216
M4	2.220	0.607	1.092	0.365	7.848	1.111	12.5	12.243
S1	0.049	0.048	0.464	0.102	17.778	2.381	5.0	5.094
S2	0.043	0.039	0.220	0.110	4.939	4.167	5.8	7.102
S3	0.042	0.021	0.252	0.202	12.057	7.143	8.0	6.558
S4	0.028	0.028	0.336	0.100	15.966	2.273	5.5	5.029

Table 3. Strouhal number of evolved creatures.

Name	Frequency (Hz)	Amplitude (m)	Speed (m/s)	St
H1	1.136	2.43	15.0	0.184
H2	0.806	2.82	14.0	0.162
H3	1.000	3.30	15.0	0.220
H4	1.250	2.60	13.5	0.241
M1	1.923	0.96	12.0	0.154
M2	2.083	1.10	14.0	0.164
M3	2.083	0.99	12.0	0.172
M4	1.111	1.07	12.5	0.095
S1	2.381	0.37	5.0	0.176
S2	4.167	0.19	5.8	0.137
S3	7.143	0.22	8.0	0.196
S4	2.273	0.30	5.5	0.124

6.1 Flight Stability

Stability is usually assumed to be problematic, especially in flapping flight, and it is sometimes suggested that it presented a particular hurdle in evolution. But there is nothing inherently destabilizing about flapping. Faster wingbeats simply amplify any existing stability or instability, and under some circumstances flapping can actually enhance stability, compared to gliding at the same airspeed [49]. It is even reasonable to apply the requirements for passive stability of gliding to flapping flight with regular wingbeats: by means of a quasi-static assumption, the net aerodynamic forces can be taken to be the same.

In our flying creatures, stability seems to evolve naturally because the creatures have to fly faster than the minimum-power speed ($V \geq V_{mp}$), and the creature inevitably drops at the start of the simulation and must stabilize the resulting oscillation in order to survive. Across a certain range of power outputs, there exist two equilibrium flight speeds for any given power (because the curve is U-shaped). Disturbances from equilibrium will only be opposed if the slope of the curve is positive (i.e., if the power required increases with flight speed); so only the higher of each pair of equilibrium speeds is stable [49].

The wing usually contributes to stability if its aerodynamic center lies behind or above the center of gravity [53]. The stability gained when the aerodynamic center lies behind the center of gravity is similar to that provided by the tailplane of a conventional aircraft. When the lift acts behind the center of gravity, the increase in lift resulting from a rising nose will tend to bring the nose back down again. The *pendulum stability* provided by having the center of gravity beneath the aerodynamic center is

Table 4. Collected morphological data on birds [29–31], with observed and calculated speeds. The data is sorted by mass.

Species	V_{mp} (m/s)	V_{obs}	Mass (kg)	Span (m)	S_b (m ²)	V_{obs}/V_{mp}
Zebra finch	5.7796	6.0	0.0136	0.3400	0.0005	1.0381
Tree swallow	6.7864	11.3	0.0201	0.3200	0.0006	1.6650
Chaffinch	7.8221	15.3	0.0228	0.2620	0.0006	1.9560
Storm petrel	7.3401	10.4	0.0350	0.3960	0.0009	1.4168
Starling	10.1526	17.3	0.0884	0.3840	0.0016	1.7039
American kestrel	8.9328	9.1	0.0900	0.5020	0.0016	1.0187
Northern flicker	10.0699	12.7	0.1320	0.5100	0.0021	1.2611
Antarctic prion	9.5211	11.1	0.1550	0.6350	0.0023	1.1658
Sparrowhawk	10.4966	8.72	0.1960	0.6110	0.0027	0.8307
Eurasian kestrel	9.8062	8.1	0.2130	0.7400	0.0029	0.8260
Black-headed gull	9.4171	10.1	0.2800	0.9630	0.0035	1.0725
Black skimmer	9.5039	9.9	0.3000	0.9900	0.0036	1.0416
Laughing gull	9.5696	9.5	0.3250	1.0300	0.0038	0.9927
Little blue heron	9.9595	8.8	0.3400	0.9800	0.0039	0.8835
Common gull	9.6168	11.6	0.3640	1.1000	0.0041	1.2062
Kittiwakes	10.4794	13.1	0.3870	0.9650	0.0043	1.2500
Arctic skua	10.0723	13.3	0.3900	1.0500	0.0043	1.3204
Common puffin	14.0241	17.6	0.3980	0.5490	0.0044	1.2549
Cape pigeon	11.2917	12.3	0.4180	0.8750	0.0045	1.0892
Royal tern	10.2423	10.0	0.4700	1.1500	0.0049	0.9763

Table 4. (continued)

Species	V_{mp} (m/s)	V_{obs}	Mass (kg)	Span (m)	S_b (m ²)	V_{obs}/V_{mp}
Wood pigeon	12.8953	15.4	0.4950	0.7510	0.0050	1.1942
Hooded crow	12.0567	10.5	0.5530	0.9250	0.0054	0.8708
Razorbill	14.8171	16.0	0.6200	0.6610	0.0059	1.0798
Widgeon	14.2827	17.1	0.7700	0.8220	0.0068	1.1972
Northern fulmar	12.4146	13.0	0.8150	1.1300	0.0070	1.0471
Red kite	10.9317	7.9	0.8510	1.5000	0.0073	0.7226
Great egret	11.6693	10.6	0.8740	1.3400	0.0074	0.9083
White ibis	13.9879	12.9	0.9000	0.9510	0.0075	0.9222
Herring gull	11.8479	11.8	0.9250	1.3500	0.0077	0.9959
Guillemot	16.5182	19.1	0.9500	0.7070	0.0078	1.1562
Common buzzard	12.2884	9.31	0.9640	1.2900	0.0079	0.7576
Grey heron	11.9028	11.0	1.2100	1.6000	0.0092	0.9241
Roseate spoonbill	13.7926	11.9	1.3000	1.2500	0.0096	0.8627
Great skua	13.3416	14.9	1.3500	1.3700	0.0099	1.1168
Eider	15.9451	20.2	1.3900	0.9780	0.0101	1.2668
Cormorant	14.7108	14.5	1.4100	1.1600	0.0102	0.9856
Magnificent frigate bird	10.6165	9.3	1.4700	2.2900	0.0105	0.8759
Osprey	12.7985	10.6	1.4900	1.5900	0.0106	0.8282
Black-backed gull	12.5816	12.8	1.5100	1.6600	0.0106	1.0173
Turkey vulture	12.3611	10.6	1.5500	1.7500	0.0108	0.8575

Table 4. (continued)

Species	V_{mp} (m/s)	V_{obs}	Mass (kg)	Span (m)	S_b (m ²)	V_{obs}/V_{mp}
Shag	16.8858	15.4	1.8100	1.0400	0.0120	0.9120
Great blue heron	13.2381	9.4	1.9200	1.7600	0.0125	0.7100
Black vulture	15.3545	10.8	2.0800	1.3800	0.0132	0.7033
Great white heron	13.8771	11.0	2.5000	1.9100	0.0149	0.7926
Cormorant	16.6373	15.0	2.5600	1.3500	0.0152	0.9015
Northern gannet	15.0009	14.9	3.0100	1.8500	0.0169	0.9932
Black-browed albatross	13.8935	13.3	3.0800	2.1900	0.0171	0.9572
Giant petrel	14.8606	15.2	3.2400	1.9800	0.0177	1.0228
Brown pelican	14.1211	10.1	3.3900	2.2600	0.0183	0.7152
Bald eagle	15.7945	11.2	4.6800	2.2400	0.0227	0.7091
Wandering albatross	16.6582	15.0	8.5500	3.0100	0.0339	0.9004
Mute swan	19.3507	16.0	9.0100	2.3100	0.0351	0.8268

similar to the self-righting property of a ship [22] and is the source of stability in parachutes and paragliders. These simple contributions are potentially included in the genotype description by allowing a variable wing root position so that the relative position of the aerodynamic center can vary. Stability is also affected by changes to the morphology of the wing, which change its sweep.

A simple experiment for observing flight stability was performed with the medium creatures. They were given disturbing moments about their pitch and roll axes. Either a pitch-up or a pitch-down moment was exerted on each creature’s central body for 10 time steps. Although it is desirable that the disturbance should be proportional to the creature’s moment of inertia, we applied the same amount (10 N·m) to all creatures, on the basis that their size and mass are similar. Figure 18 is a qualitative overview of some creatures’ motion, visualized as wingtip trajectories, which show the aerodynamic center position relative to the center of mass. Creatures were placed in the air with no gravity. All except M1 showed pitch-down movements, showing that the aerodynamic center is behind the center of gravity. M2 generated the strongest pitch-down movement, and even M1’s pitch-up movement was very slight. The flapping of M3 and M4 generated more thrust than the others.

Figures 19 and 20 show the flight profiles after the disturbance. In all cases, this looks like a damped oscillation. It is strange that the rising height of M1 (which seems most unstable after the pitch-up disturbance) is very small at the time of the pitch-up disturbance, but this is because M1 did

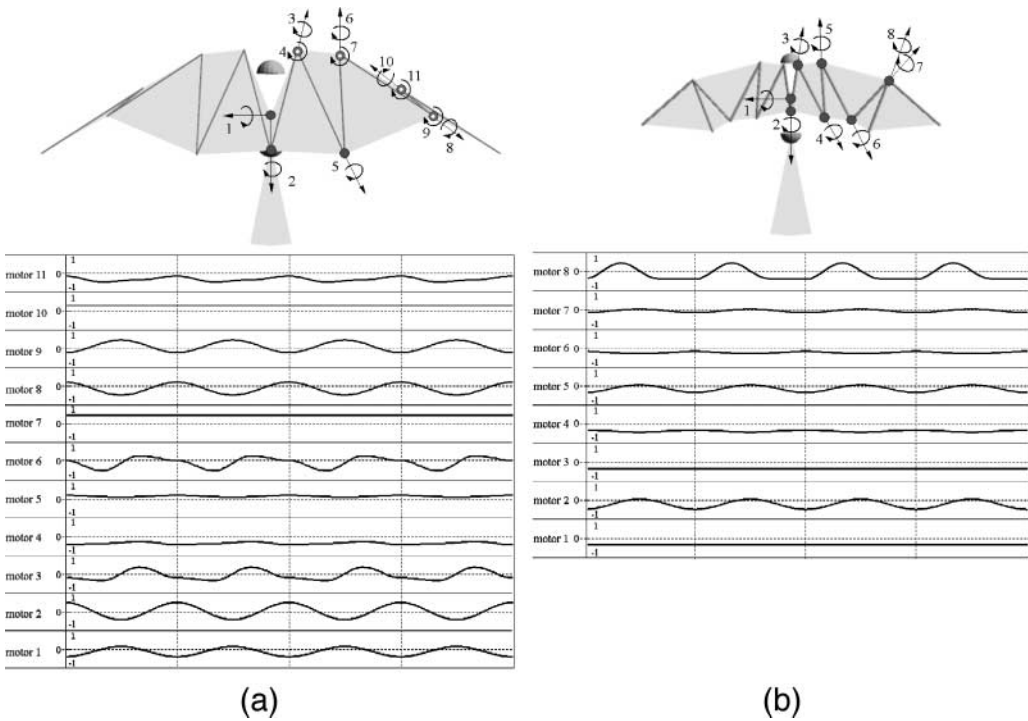


Figure 17. Example of motor controllers. H3 and M3, with the richest movements of their joint motors, are described. Four cycle periods are plotted for each controller. H3 has four joints with two degrees of freedom, but M3 only has joints with one degree of freedom.

a somersault. M3 and M4 have more thrust and show better stability. Higher thrust allows the necessary stabilizing forces to be generated more quickly.

The roll disturbances were exerted during one time step. Figure 21 shows consecutive images of the response by M3 to three different roll impacts. Figure 22 shows the different responses of M1, M2, and M4 to the same disturbance (100 N·m). Here, there is both pendulum stabilization and stabilization through the dihedral effect [9, 26]. If the left wing of a creature is raised, the net lift vector does not remain vertical, so the weight now has a component in the direction of the right

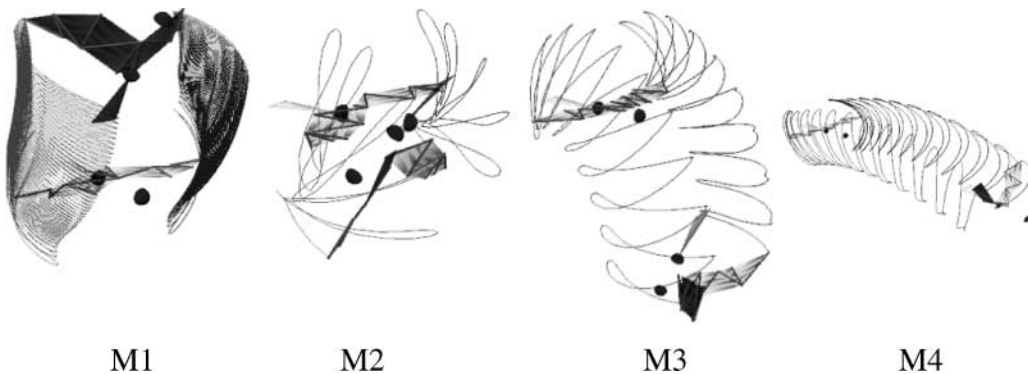


Figure 18. Brief visualization of the aerodynamic center of the creatures. Creatures were placed in the air with no gravity, and their trajectories are shown. All except M1 showed pitch-down movement (aerodynamic center is behind the center of gravity). The two on the right show stronger thrust.

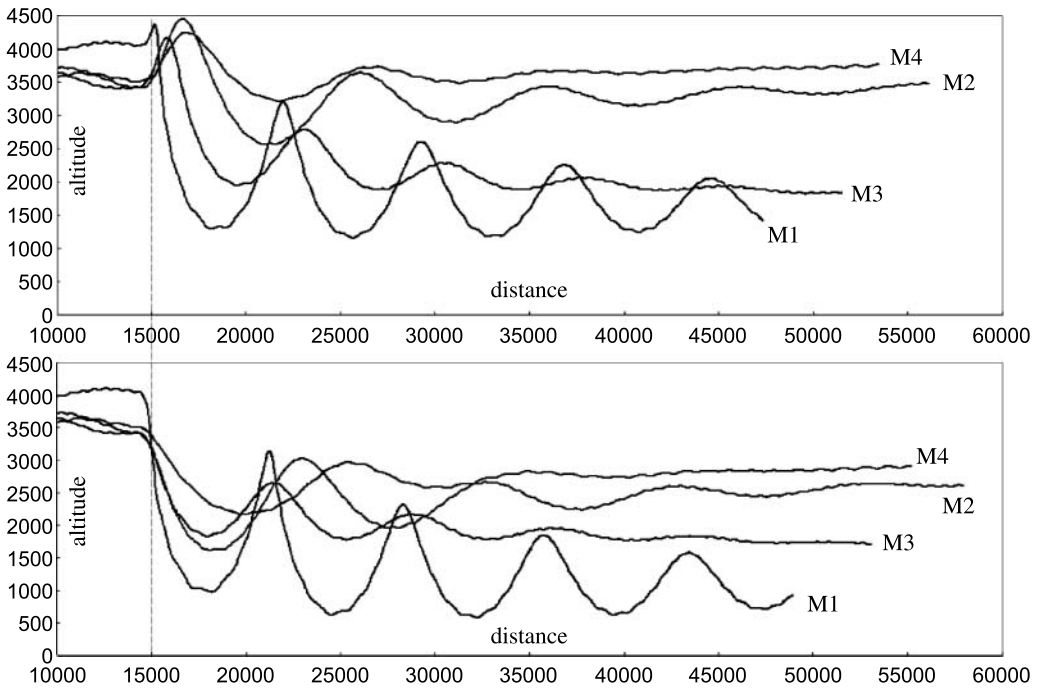


Figure 19. Oscillations after a pitch disturbance. The upper image shows the aftermath of a pitch-up disturbance, while the lower image shows the result of pitch-down. The graphs represent 2000 time steps and were aligned at the start of disturbance, represented by a dashed line. The units are centimeters.

wing. The body begins to slide down in the direction of the right wing. Because of the upward dihedral angle of the wings, this sideslip increases the angle of attack of the right wing and decreases the angle of attack of the left wing. The higher lift on the right wing produces a stabilizing moment. In Figure 22a, M2 makes a strong initial downstroke and returns to a safe roll angle more quickly than the other creatures, performing a large flat spiral and losing little altitude, though the final

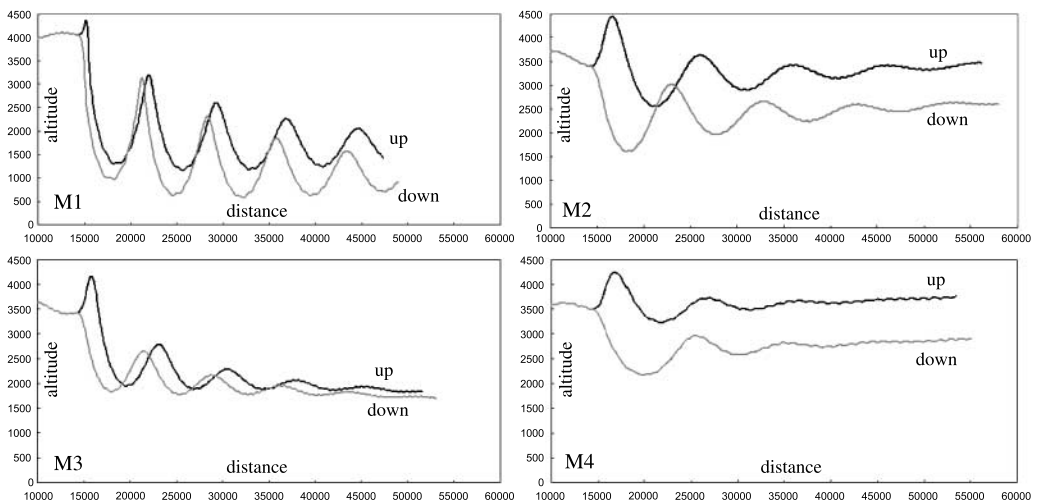


Figure 20. Trajectories of each creature. Each figure shows the response after pitch-up (black line) and pitch-down (gray line) impacts. The two cases show similar stabilization trajectories.

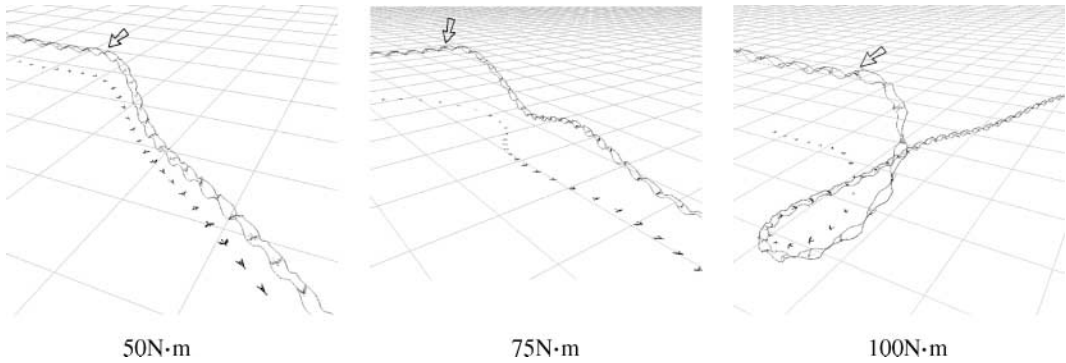


Figure 21. Stabilization after receiving different amounts of roll disturbance. The arrow indicates the time of impact.

recovery is slow because of its small sideslip. Figure 22b shows the spiral descent of M1, which has a typical, moderate level of stability. M4 (Figure 22c) is very unstable in this test, though it showed the best pitch stability. It seems that its wingbeat frequency is too low and its amplitude is too high; the creature simply rolled over before being able to make the next downstroke.

Both pitch and roll stability are achieved by appropriate coupling of several effects. In all cases, however, the pendulum effect is a necessary condition for better stability, because it not only helps a creature to stabilize, but also significantly extends the allowable error limits for the magnitude of stabilizing moments, which are produced by the relative position of the aerodynamic center or by the dihedral effect. Without the pendulum effect, there could hardly be any roll stabilization, although pitch stability could still be achieved by having sufficient sweep of wings and a strong thrust.

6.2 The Strouhal Number in Cruising Flight

We now analyze our results in terms of the Strouhal number when cruising. For dolphins, sharks, and other bony fish traveling at their preferred cruising speed, the ratio of the product of tail frequency and amplitude to forward speed is constrained for efficiency to a narrow range of values. This dimensionless ratio is the Strouhal number, and evolution seems to favor efficient swimming motion with a Strouhal number in the range 0.2 to 0.4. A recent study by Taylor et al. [50] showed that Strouhal numbers for birds, bats, and insects flying at cruising speed also seem to be constrained within a similar range of values. It is surprising to see the same range of values across creatures in such different habitats, with wildly different size, mass, and flight patterns, as well as across species that evolved the ability to fly independently.

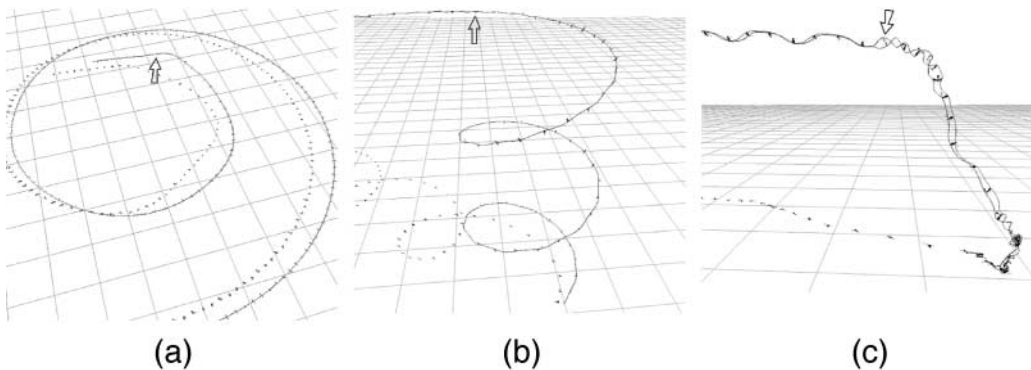


Figure 22. Response patterns to a roll disturbance. (a) Large planar spiral path, which results from slow stabilization. (b) Falling spiral. (c) Crash.

For an animal in flight, the Strouhal number is determined by the wingbeat frequency (f), multiplied by the amplitude (A) of the wing stroke, divided by the animal's forward speed (U) through the air:

$$St = \frac{fA}{U}. \tag{15}$$

Also known as wingtip excursion, the amplitude of the stroke is the vertical distance traveled by the tip of the wing during the flapping stroke.

In terms of fluid dynamics, the Strouhal number is concerned with the number of vortices shed by an oscillating object in the fluid [10]. While detailed fluid behavior of this sort is not captured by our simplified aerodynamics, we consider the Strouhal number to be relevant because formalized aerodynamics such as thin airfoil theory and lifting-line theory encapsulate the effects of those complicated phenomena. The Strouhal number is bound to affect aerodynamic force coefficients and propulsive efficiency, because it defines the maximum aerodynamic angle of attack and the time scales associated with the growth and shedding of vortices, which are the source of aerodynamic forces.

The significance of Strouhal numbers in the range 0.2 to 0.4 can be explained in terms of the optimal space-time synchronization of an oscillating foil so that it sheds a fully developed vortex at each end of each downstroke. Therefore the propulsive efficiency of a flapping foil usually peaks in this range. If the Strouhal number is too small, the vortex is shed before the end of downstroke; if it is too large, the vortex collides with the foil on the upstroke. Although these phenomena were not modeled in our work, we suggest that the lift/drag coefficient, the fitness constraints, and the creature morphology involved in the evolution process delineate three boundaries on feasible operation: the minimum-power speed roughly bounds the speed range, the minimum undulatory movement of the body prevents the wingbeat from being too slow or having too high an amplitude, and the reward for low power consumption limits rapid change of wing motion, which would lead to excessive frequency and low amplitude.

Figure 23 shows the Strouhal numbers of actual birds, as presented by Taylor, together with those of our evolved creatures (see Table 3). The evolved creatures show a similar range to the real animals.

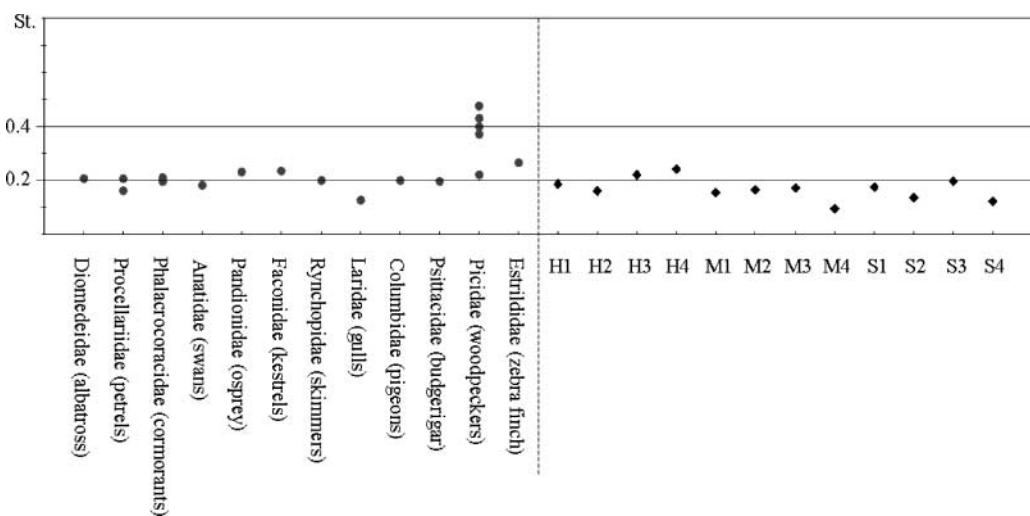


Figure 23. Strouhal numbers for birds from Taylor (some have multiple values) and for the creatures in this work. All data from Taylor is for continuous flight, except for budgerigars and woodpeckers, for which it is for intermittent flight.

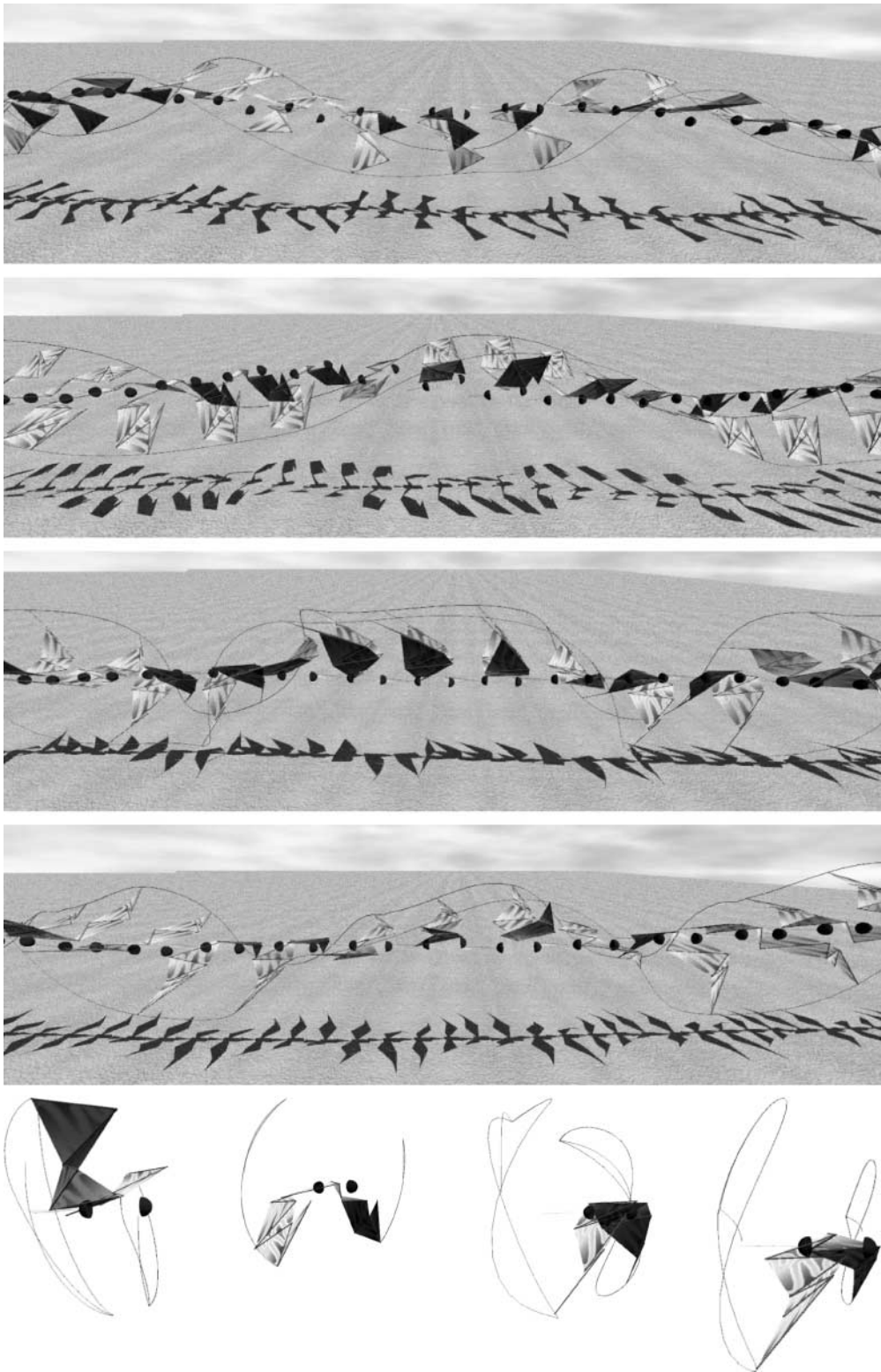


Figure 24. Consecutive images of the flight of the heavy creatures. From the top, H1, H2, H3, and H4 are shown, sampled every 10 frames. The four images at the bottom show the wingtip trajectory of each creature.

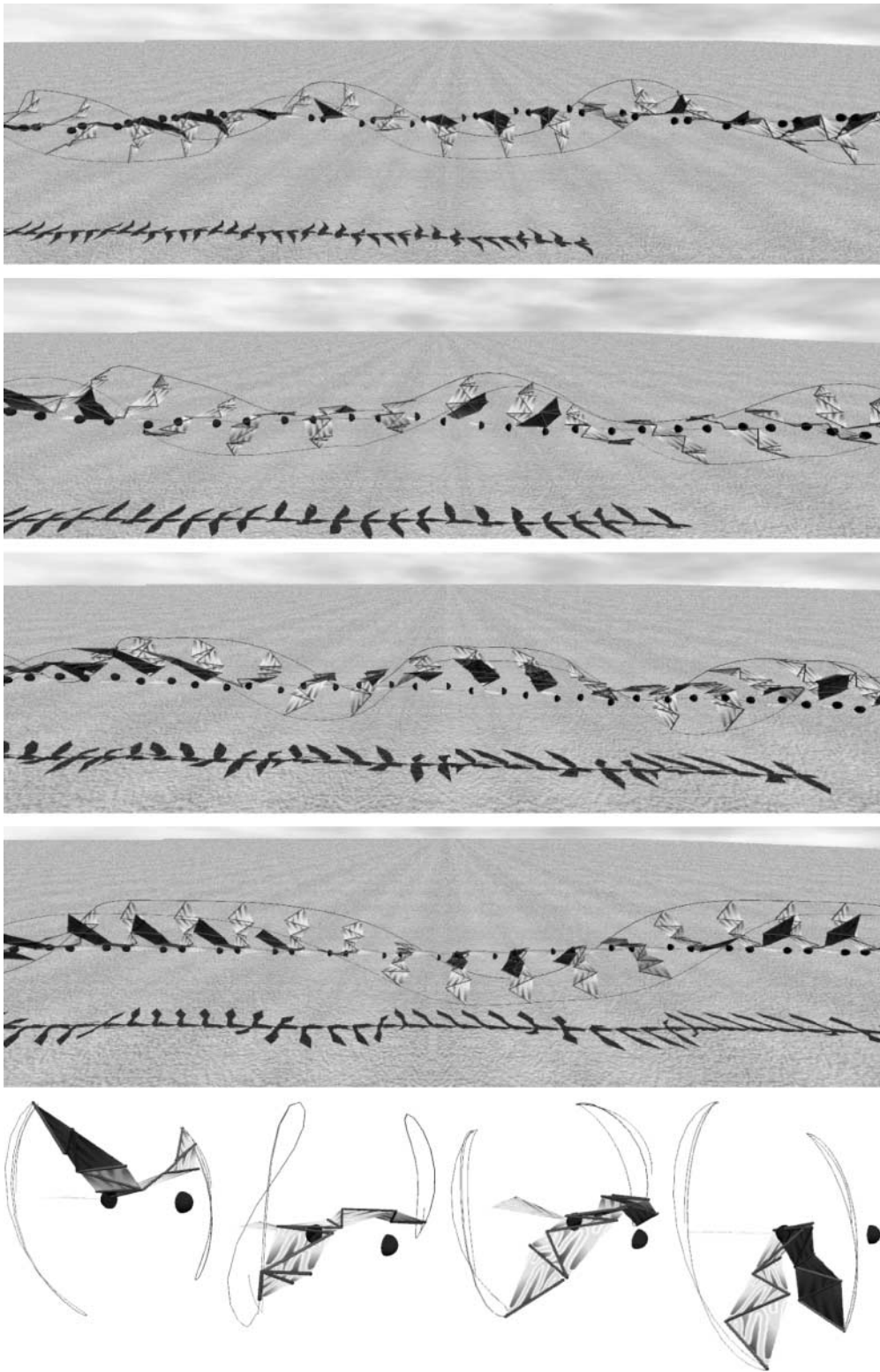


Figure 25. Consecutive images of the flight of the medium creatures. From the top, M1, M2, M3, and M4 are shown, sampled every 5 frames.

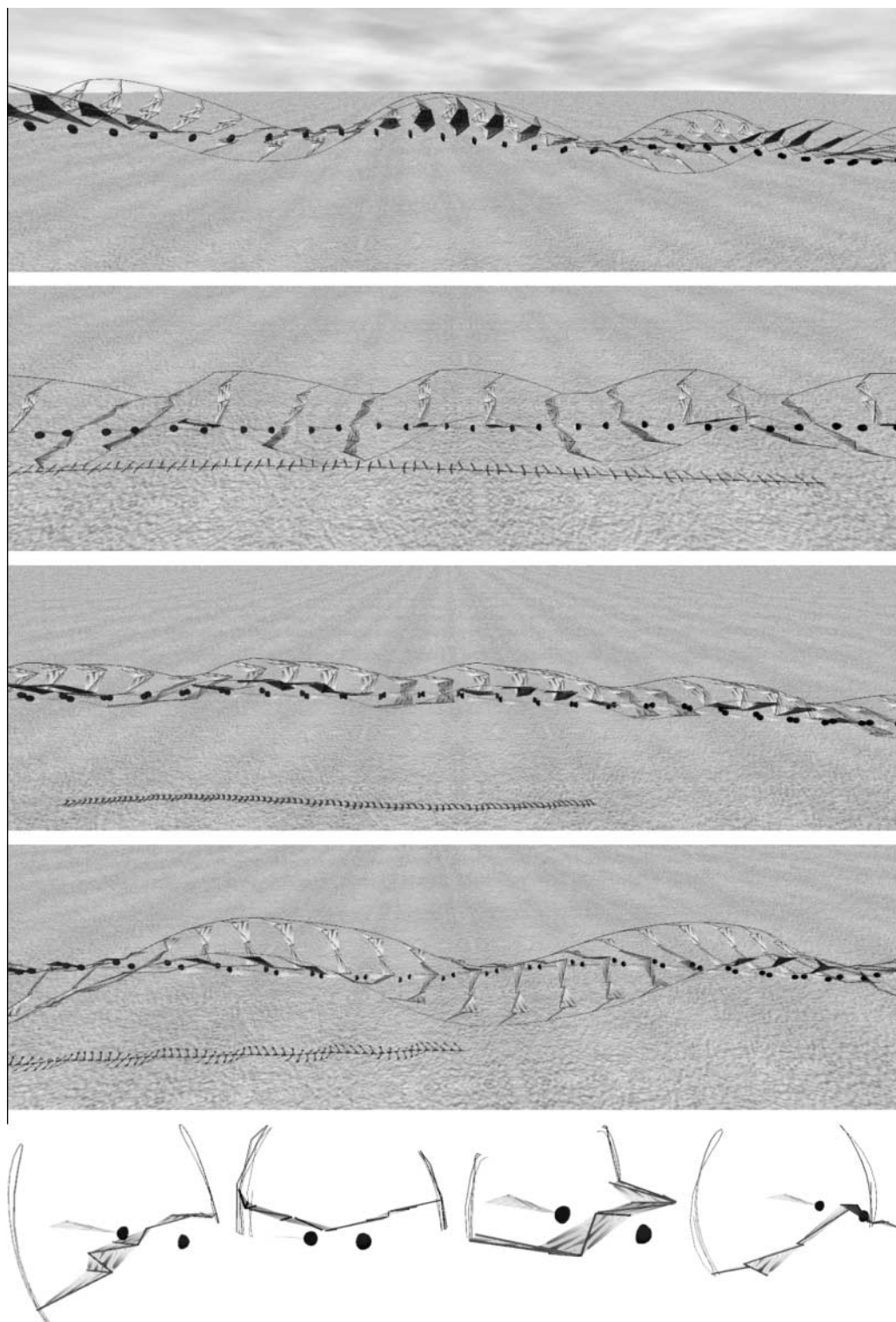


Figure 26. Consecutive images of the flight of the small creatures. From the top, S1, S2, S3, and S4 are shown, sampled every 2 frames.

In Taylor's measurements, birds have lower values within the range and bats have higher values. Our creatures incorporate many parameters from birds, and also have low values.

7 Conclusions and Future Work

We have presented an evolutionary approach to evolve both wing morphology and flapping flight, which is a challenging topic in the generation of virtual creatures. We combined several aspects of aerodynamics and flight energetics with morphological characteristics within an evolutionary framework, and attempted to include intrinsic flight stability indirectly in the evolution system. The resulting creatures have enhanced physical and biological plausibility.

Nevertheless, there are several sources of physical inaccuracy, especially the lack of unsteady-state aerodynamic effects, of allowance for interactions between wing segments, and of a model of the spanwise force distribution, which are hard to achieve with an arbitrary wing shape and motion. A major key to success in this sort of evolutionary system is the availability of sufficiently accurate physics of the environment (even in the generation of swimming and crawling creatures). Therefore more computationally efficient and sophisticated aerodynamic influences need to be modeled if we are to improve on the results reported in this article.

There are significant constraints on the ways in which a bird may move its wings [37], and it would be interesting to explore possible modes of flight more widely, by excluding biological soundness and loosening the mechanical constraints on a creature's body, without abandoning physical accuracy. We expect that the search space for powered flight is probably quite small and also discontinuous, because we see that most flying animals have several significantly different modes of flight (such as gliding or flapping, with continuous or intermittent wingbeats).

The next step will be to generate stable and continuous flight maneuvers by our enhanced flying creatures. Achieving a flexible and robust maneuvering capability is likely to require both passive stability and the use of dynamic neural networks. In previous work [42] we attempted to generate maneuvering creatures using traditional artificial neural networks, but the maneuvers were restricted to a given path, and the creatures were controlled by static networks, which were unable to respond to external disturbances, leading to high instability. We plan to replace our sinusoidal controller with central pattern generators [3, 7, 18, 19], and achieve navigation using CTRNNs. Another interesting goal would be to generate a wider range of behaviors, which could be totally changed as required, and not simply modulated. In an eventful environment, a creature would be able to select its mode of flight between the translatory mode and the stationary mode (soaring in a rising current or diving toward a prey). Applying selective attention behavior [11, 45] to this might be a good initial target.

Bringing evolved flyers into the real world is not an impossible suggestion. A robot vehicle would be thrown into an environment that is more unstable and noisy than any we can model, but we believe that adaptive control could bridge the reality gap.

Acknowledgments

Thanks to adviser Chang-Hun Kim for support and help with this article, and Russell Smith for sharing his ODE engine. Special thanks to John Woodwark for his delicate correction and continuous feedback on this article. This work was supported by a Korea Research Foundation Grant (KRF-2003-041-D20461), the Korea Science and Engineering Foundation in the Ministry of Science & Technology (R01-2005-000-10120-0), and the University IT Research Center Project.

References

1. Anitescu, M., & Potra, F. A. (1997). Formulating rigid multi-body dynamics with contact and friction as solvable linear complementarity problems. *Nonlinear Dynamics*, 14, 231–247.
2. Augustsson, P., Wolff, K., & Nordin, P. (2002). Creation of a learning, flying robot by means of evolution. *Proceedings of the Genetic and Evolutionary Computation Conference (GECCO 2002)* (pp. 1279–1285). New York: Morgan Kaufmann.

3. Beer, R. D., Chiel, H. J., & Gallagher, J. C. (1999). Evolution and analysis of model CPGs for walking II. General principles and individual variability. *Journal of Computational Neuroscience*, 7(2), 119–147.
4. Beer, R. D. (1995). On the dynamics of small continuous-time recurrent neural networks. *Adaptive Behavior*, 3(4), 471–511.
5. Beer, R. D. (1996). Toward the evolution of dynamical neural networks for minimally cognitive behavior. *From Animals to Animats 4: Proceedings of the Fourth International Conference on Simulation of Adaptive Behavior* (pp. 421–429). Cambridge, MA: MIT Press.
6. Bongard, J. C., & Paul, C. (2000). Investigating morphological symmetry and locomotive efficiency using virtual embodied evolution. *From Animals to Animats 6: Proceedings of the Sixth International Conference on the Simulation of Adaptive Behavior*. Cambridge, MA: MIT Press.
7. Chiel, H. J., Beer, R. D., & Gallagher, J. C. (1999). Evolution and analysis of model CPGs for walking I. Dynamical modules. *Journal of Computational Neuroscience*, 7(2), 99–118.
8. Collins, S. H., Wisse, M., & Ruina, A. (2001). A three-dimensional passive-dynamic walking robot with two legs and knees. *The International Journal of Robotics Research*, 20(7), 607–615.
9. Etkin, B., & Reid, L. D. (1996). *Dynamics of flight: Stability and control* (3rd ed.). New York: Wiley.
10. Fox, R. W., & McDonald, A. T. (1976). *Introduction to fluid mechanics* (5th ed.). New York: Wiley.
11. Gallagher, J. C., & Beer, R. D. (1999). Evolution and analysis of dynamical neural networks for agents integrating vision, locomotion and short-term memory. *Proceedings of the Genetic and Evolutionary Computation Conference (GECCO-99)* (pp. 1273–1280).
12. Goldstein, S. (1942). Approximate two-dimensional aerofoil theory: Part 1: Velocity distributions for symmetrical aerofoils (CP-68). British Aeronautical Research Council.
13. Greenewalt, C. H. (1962). Dimensional relationships for flying animals. *Smithson Miscellaneous Collection*, 1962(144), 1–46.
14. Greenewalt, C. H. (1975). The flight of birds. *Transactions of the American Philosophical Society*, 1975(65), 1–67.
15. Hedenstrom, A., & Alerstam, T. (1995). Optimal flight speed of birds. *Philosophical Transactions of the Royal Society of London B*, 348(47), 471–487.
16. Houston, A. I. (1992). Optimization of locomotion. In R. McN. Alexander (Ed.), *Mechanics of animal locomotion, advances in comparative environmental physiology* (pp. 277–300). Berlin: Springer.
17. Husbands, P. (2003). *Lecture notes for adaptive systems*. University of Sussex, UK.
18. Ijspeert, A. J., Hallam, J., & Willshaw, D. (1998). Evolution of a central pattern generator for the swimming and trotting gaits of the salamander. *Proceedings of the Third International Conference on Computational Intelligence & Neurosciences (ICCN98)* (pp. 24–38).
19. Ijspeert, A. J., Hallam, J., & Willshaw, D. (1998). From lampreys to salamanders: Evolving neural controllers for swimming and walking. *From Animals to Animats 5: Proceedings of the Fifth International Conference on the Simulation of Adaptive Behavior (SAB98)* (pp. 390–399). Cambridge, MA: MIT Press.
20. Klein, J. (2002). Breve: A 3D environment for the simulation of decentralized systems and artificial life. *ALife VIII: Proceedings of the Eighth International Conference on the Simulation and Synthesis of Living Systems*. Cambridge, MA: MIT Press.
21. Komosinski, M., & Ulatowski, S. (1999). Framsticks: Towards a simulation of a nature-like world, creatures and evolution. *Advances in Artificial Life: Proceedings of the Fifth European Conference on Artificial Life* (pp. 261–265). Berlin: Springer-Verlag.
22. Lighthill, J. (1974). Aerodynamic aspects of animal flight: Fifth fluid science lecture at the Royal Institution. *Bulletin of the Institute of Mathematics and its Applications*, 10, 363–393.
23. Lipson, H., & Pollack, J. B. (2000). Automatic design and manufacture of robotic life-forms. *Nature*, 406, 974–978.
24. McCormick, B. W. (1979). *Aerodynamics, aeronautics, and flight mechanics*. New York: Wiley.
25. Milano, M., Giannakopoulos, X., Koumoutsakos, P., & Schmidhuber, J. (2000). Evolving strategies for active flow control. *Proceedings of the IEEE Congress on Evolutionary Computation 2000 (CEC'00)*, 2, 212–218.

26. Nelson, R. C. (1998). *Flight stability and automatic control* (2nd ed.). New York: WCB McGraw-Hill.
27. Pennycuik, C. J. (1975). Mechanics of flight. *Journal of Avian Biology*, 5, 1–75.
28. Pennycuik, C. J. (1989). *Bird flight performance: A practical calculation manual*. Oxford, UK: Oxford University Press.
29. Pennycuik, C. J. (1996). Wingbeat frequency of birds in steady cruising flight: New data and improved predictions. *The Journal of Experimental Biology*, 199, 1613–1618.
30. Pennycuik, C. J. (1997). Actual and optimum flight speeds: Field data reassessed. *The Journal of Experimental Biology*, 200, 2355–2361.
31. Pennycuik, C. J. (2001). Speeds and wingbeat frequencies of migrating birds compared with calculated benchmarks. *The Journal of Experimental Biology*, 204, 3283–3294.
32. Prandtl, L. (1918). Tragflügeltheorie. I Mitteilung. *Nachrichten von der Gesellschaft der Wissenschaften zu Göttingen. Mathematisch-Physikalische Klasse*, 151.
33. Prandtl, L. (1919). Tragflügeltheorie. II Mitteilung. *Nachrichten von der Gesellschaft der Wissenschaften zu Göttingen. Mathematisch-Physikalische Klasse*, 107.
34. Ramakrishnananda, B., & Wong, K. C. (1999). Animating bird flight using aerodynamics. *The Visual Computer*, 15(10), 494–508.
35. Ray, T. S. (2000). Aesthetically evolved virtual pets. *Artificial Life VII Workshop Proceedings* (pp. 158–161). Portland, OR: Reed College.
36. Rayner, J. M. V. (1985). Bounding and undulating flight in birds. *Journal of Theoretical Biology*, 117, 47–77.
37. Rayner, J. M. V. (2001). Mathematical modeling of the avian flight power curve. *Mathematical Methods in the Applied Sciences*, 24, 1485–1514.
38. Rayner, J. M. V., Viscardi, P. W., Ward, S., & Speakman, J. R. (2001). Aerodynamics and energetics of intermittent flight in birds. *American Zoologist*, 41(2), 188–204.
39. Reynolds, C. W. (1987). Flocks, herds, and schools: A distributed behavioral model. *ACM Computer Graphics*, 21(4), 25–34.
40. Rosenberg, S. (2001). Evolving responsively: Adaptive mutation. *Nature Reviews Genetics*, 2, 504–515.
41. Shim, Y. S., & Kim, C. H. (2003). Generating flying creature using body-brain coevolution. *Proceedings of ACM SIGGRAPH/Eurographics Symposium on Computer Animation* (pp. 276–285).
42. Shim, Y. S., Kim, S. J., & Kim, C. H. (2004). Evolving flying creatures with path-following behavior. *ALife IX: Proceedings of the 9th International Conference on the Simulation and Synthesis of Living Systems* (pp. 125–132). Cambridge, MA: MIT Press.
43. Sims, K. (1994). Evolving 3D morphology and behavior by competition. *ALife IV: Proceedings of the Fourth International Workshop on the Synthesis and Simulation of Living Systems* (pp. 28–39). Cambridge, MA: MIT Press.
44. Sims, K. (1994). Evolving virtual creatures. *ACM Computer Graphics (SIGGRAPH '94)* (pp. 15–22).
45. Slocum, A. C., Downey, D. C., & Beer, R. D. (2000). Further experiments in the evolution of minimally cognitive behavior: From perceiving affordances to selective attention. *From Animals to Animats 6: Proceedings of the Sixth International Conference on Simulation of Adaptive Behavior* (pp. 430–439). Cambridge, MA: MIT Press.
46. Smith, R. (1998). *Intelligent motion control with an artificial cerebellum*. Unpublished doctoral dissertation, University of Auckland, New Zealand. Available online, including ODE engine, at <http://ode.org>.
47. Spedding, G. R., & Pennycuik, C. J. (2001). Uncertainty calculations for theoretical flight power curves. *Journal of Theoretical Biology*, 208, 127–139.
48. Stewart, D. E., & Trinkle, J. C. (1996). An implicit time-stepping scheme for rigid-body dynamics with inelastic collisions and Coulomb friction. *International Journal of Numerical Methods in Engineering*, 39, 2673–2691.
49. Taylor, G. K., & Thomas, A. L. R. (2002). Animal flight dynamics II: Longitudinal stability in flapping flight. *Journal of Theoretical Biology*, 214, 351–370.

50. Taylor, G. K., Nudds, R. L., & Thomas, A. L. R. (2003). Flying and swimming animals cruise at a Strouhal number tuned for high power efficiency. *Nature*, *425*, 707–711.
51. Taylor, T., & Massey, C. (2001). Recent developments in the evolution of morphologies and controllers for physically simulated creatures. *Artificial Life*, *7*(1), 77–87.
52. Tennekes, H. (1996). *The simple science of flight: From insects to jumbo jets*. Cambridge, MA: MIT Press.
53. Thomas, A. L. R., & Taylor, G. K. (2001). Animal flight dynamics I: Stability in gliding flight. *Journal of Theoretical Biology*, *212*, 399–424.
54. Vaughan, E. D., Paolo, E. D., & Harvey, I. R. (2004). The evolution of control and adaptation in a 3D powered passive dynamic walker. *ALife IX: Proceedings of the Ninth International Conference on the Simulation and Synthesis of Living Systems* (pp. 139–145). Cambridge, MA: MIT Press.
55. Ventrella, J. (1994). Explorations in the emergence of morphology and locomotion behavior in animated characters. *ALife IV: Proceedings of the Fourth International Workshop on the Synthesis and Simulation of Living Systems* (pp. 436–441). Cambridge, MA: MIT Press.
56. Ventrella, J. (1998). Attractiveness vs. efficiency: How mate preference affects locomotion in the evolution of artificial swimming organisms. *ALife VI: Proceedings of the Sixth International Conference on Artificial Life* (pp. 178–186). Cambridge, MA: MIT Press.
57. Weis-Fogh, T., & Jensen, M. (1956). Biology and physics of locust flight I: Basic principles in insect flight. A critical review. *Philosophical Transactions of the Royal Society of London B*, *239*, 415–458.
58. Wu, X. C., & Popović, Z. (2003). Realistic modeling of bird flight animations. *Proceedings of SIGGRAPH 2003* (pp. 888–895). New York: ACM.

Copyright of Artificial Life is the property of MIT Press and its content may not be copied or emailed to multiple sites or posted to a listserv without the copyright holder's express written permission. However, users may print, download, or email articles for individual use.